Changes in cerebellar protein expression and Purkinje cell excitability by cerebellum-dependent motor learning

소뇌−의존적 운동 학습에 의해 유도된 소뇌
단백질 발현과 퍼킨지 세포 흥분성의 변화

2021년 8월

서울대학교 대학원

의과학과 의과학전공

김 용 규

Ph.D Dissertation of Biomedical Sciences

소뇌−의존적 운동 학습에 의해 유도된 소뇌 단백질 발현과 퍼킨지 세포 흥분성의 변화

Changes in cerebellar protein expression and Purkinje cell excitability by cerebellum-dependent motor learning

August 2021

Major in Biomedical Sciences

Department of Biomedical Sciences

Seoul National University

Graduate School

Yong Gyu Kim

소뇌−의존적 운동 학습에 의해 유도된 소뇌 단백질 발현과 퍼킨지 세포 흥분성의 변화

지도 교수 김 상 정

이 논문을 의학박사 학위논문으로 제출함

2021년 4월

서울대학교 대학원
의과학과 의과학전공

김 용 규

김용규의 의학박사 학위논문을 인준함

2021년 7월

위원장 ＿＿＿＿＿＿＿＿＿＿

부위원장 ＿＿＿＿＿＿＿＿＿＿

위원 ＿＿＿＿＿＿＿＿＿＿

위원 ＿＿＿＿＿＿＿＿＿＿

위원 ＿＿＿＿＿＿＿＿＿＿

Changes in cerebellar protein expression and Purkinje cell excitability by cerebellum-dependent motor learning

**A Dissertation Submitted to the Faculty of the Department of Biomedical Sciences
at
Seoul National University
by**

Yong Gyu Kim

in Partial Fulfillment of the Requirements for the Degree of Doctor of Philosophy

**Advisor: Sang Jeong Kim
April 2021**

**Approved by Thesis Committee:
July 2021**

Chair   _____

Vice Chair   _____

Examiner   _____

Examiner   _____

Examiner   _____

PREFACE

This Ph.D dissertation written by Yong Gyu Kim contains two chapters. Chapter I is adopted from the previously published article in Journal of Proteome Research (Kim YG, Woo J, Park J, Kim S, Lee YS, Kim Y, et al. *Quantitative proteomics reveals distinct molecular signatures of different cerebellum-dependent learning paradigms.* J Proteome Res. 2020;19(5):2011–25.). In addition, it is noted that the entire TMT-labeled quantification proteomics step, including proteolysis, LC-MS/MS analysis, and protein identification, was performed in collaboration with Proteomics & Biomarker Laboratory at Seoul National University (Professor Youngsoo Kim). Chapter II is partially adopted from the previously published article in Molecular Brain (Kim, Y.G., Kim, S.J. *Decreased intrinsic excitability of cerebellar Purkinje cells following optokinetic learning in mice.* Mol Brain 13, 136 (2020).).

ABSTRACT

Changes in cerebellar protein expression and Purkinje cell excitability by cerebellum-dependent motor learning

Yong Gyu Kim

Major in Biomedical Sciences

Department of Biomedical Sciences

Seoul National University

Graduate School

One of the fundamental questions in neuroscience is how the brain encodes learning and memory processes at the molecular and cellular levels. Of the various approaches to resolve this question, it is useful to investigate the molecular or cellular traces that are formed in the brain after learning in wildtype animals. In this dissertation, I attempted to find traces of cerebellum-dependent motor memory at the molecular and cellular levels in the cerebellum.

First, in chapter I, I attempted to find the trace of cerebellum-dependent motor memory at the molecular level of the cerebellum. The cerebellum improves motor performance by adjusting the motor strength appropriately. According to previous studies, it has been suggested that distinct cellular mechanisms may exist depending on the direction in which the motor strength is adjusted. Given that de novo protein synthesis is essential in the formation and retention of memory in the brain, I hypothesized that motor learning in the opposite direction would induce a distinct pattern of protein expression in the cerebellum.

I conducted quantitative proteomic profiling to compare the level of protein expression in the cerebellum at 1 and 24 h after training from mice that underwent different paradigms of cerebellum-dependent oculomotor learning from specific directional changes in motor gain. I quantified a total of 43 proteins that were

significantly regulated in each of the three learning paradigms in the cerebellum at 1 and 24 h after learning. In addition, functional enrichment analysis identified protein groups that were differentially enriched or depleted in the cerebellum at 24 h after the three oculomotor learnings, suggesting that distinct biological pathways may be engaged in the formation of three oculomotor memories. Weighted correlation network analysis discovered groups of proteins significantly correlated with oculomotor memory. Finally, four proteins (Snca, Sncb, Cttn, and Stmn1) from the protein group correlated with the learning amount after oculomotor training were validated by Western blot. This study provides a comprehensive and unbiased list of proteins related to three cerebellum-dependent motor learning paradigms, suggesting the distinct nature of protein expression in the cerebellum for each learning paradigm.

In chapter II, I focused on the optokinetic response (OKR) learning among the three oculomotor paradigms mentioned above. The OKR is a reflexive eye movement evoked by a motion of the visual field to stabilize an image on the retina. The OKR is known to adapt its strength to cope with an environmental change throughout life. The cerebellum is well-known to participate in this oculomotor learning as an adaptive controller. In the adaptive controlling unit, the Purkinje cell (PC) is known to integrate multimodal sensory information in the cerebellar cortex as the sole output of the cerebellum. Despite the significance of PC in the neural circuit modulating OKR, the electrophysiological properties of PC in optokinetic learning have not been fully understood. Therefore, in this dissertation, I examined whether changes in the intrinsic and synaptic excitability of PC is induced in mice underwent 50 min of optokinetic learning.

By utilizing the whole-cell patch-clamp recording, I compared the electrophysiological properties between the control and learned group, and found that the mean firing rate of PCs was decreased in response to intracellular depolarizing current injection and the rheobase current was increased in the learned group. In addition, I found that acute optokinetic learning induced a decrease in excitatory synaptic transmission at parallel fiber to PC synapse by reducing the presynaptic release probability. Taken together, optokinetic learning induces the suppressed neuronal excitability at both the intrinsic and synaptic factors of cerebellar PCs, suggesting the possibility of the occurrence of multiple plasticity

governing cerebellum-dependent motor learning.

In this dissertation, I conducted two independent observational studies to suggest possible molecular and cellular traces for cerebellum-dependent motor memory. Identified proteins and neural plasticity should lead us to further investigations to validate their roles in memory formation and consolidation. In conclusion, the discoveries in this dissertation would be a potentially important resource for discovering unknown molecules or plasticity mechanisms underlying cerebellum-dependent motor memory.

Keyword: Cerebellum, Cerebellum-dependent motor learning, Oculomotor learning, Proteomic profiling, Bioinformatics, Optokinetic response (OKR), Vestibulo-ocular reflex (VOR), Purkinje cell, Electrophysiology, Whole-cell patch-clamp recording, Intrinsic excitability, Synaptic transmission

Student Number: 2012-30576

Table of Contents

List of Figures and Tables

Chapter I

Chapter II

Tables

GENERAL INTRODUCTION

Learning and memory is the ability to encode and recall new information about the physical world, which is crucial for organisms to adapt and survive from the change of their environments [1]. For animals, it is vital to remember the location where food was stored or traces of predators. In humans, memory deficit has a significant impact on an individual's life [2, 3]. Given the importance of learning and memory, this cognitive function has been a major research topic in the field of neuroscience [1, 4].

Of various research fields, in particular, neurobiology has been trying to uncover the biological substance of learning and memory in the brain [5]. At the microscopic level, the brain is composed of the interconnections of neuronal and non-neuronal cells. Moreover, it is known that a number of molecules with different functions are expressed in a single neuron. Given these fundamental elements of the brain, neurobiologists questioned that memory would be encoded by persistent physical changes (hereafter memory trace) in the molecular and cellular levels [6-8].

To address this question, Observational studies are a fundamental and typical approach [5]. An observational study is to discover physical changes in brain regions that are closely related to memory in learned animals. When memory-related neurons are stimulated, activity-dependent genes are induced and de novo proteins with specific functions are synthesized, leading to memory formation and consolidation [4]. Since the high-throughput molecular profiling technique identifies and quantifies a variety of molecules at once, this approach has the advantage of discovering memory-related candidate molecules. In the hippocampus and amygdala, which are well known memory-related regions in the brain, observational studies have been largely attempted to find memory traces at the molecular level using microarray, RNA-sequencing, or mass-spectrometry-based proteomics [9-11].

In addition, it is useful to identify electrophysiological changes in memory-related neurons in order to find memory traces at the cellular level [12]. In the brain, neurons receive information via dendrites and transmit information to postsynaptic neuron via axon terminals. In this process, it is known that physiological stimulation induces

long-term plasticity of synaptic transmission or the intrinsic excitability, which are widely accepted as cellular correlates for memory formation [13-17]. In early observational studies, neurophysiologists targeted unspecified neurons in the hippocampus, amygdala, or cerebral cortex of learned animals [18-20]. Recently, they utilized advanced techniques that reliably label specific neuronal ensembles that were active during the learning period to find memory at a more specific level [21, 22].

The cerebellum is known to encode motor memory, such as the acquisition of new motor skills and fine-tuning of body movements. The classical hypothesis, namely the cerebellar LTD hypothesis, has been suggested that motor learning can be achieved by modification of the efficacy of certain synapses in the cerebellar cortex [23]. However, accumulated evidence indicates that the cerebellar LTD hypothesis cannot solely account for the underlying mechanism for cerebellum-dependent motor learning and memory, and that other neural mechanisms may be involved in motor memory formation [24, 25].

For comprehensive understanding of motor learning governed by the cerebellum and discovery of memory traces, further observational studies at the molecular or cellular level should be facilitated. Previous studies using electrophysiological approach have mainly focused on the validation of cerebellar LTD in motor learning [26-29]. In addition, the cerebellum has only recently begun testing whether the intrinsic excitability is involved in motor memory formation and consolidation [30, 31]. Furthermore, molecular profiling methods have rarely been applied in the field of cerebellum-dependent motor memory [32, 33]. Considering previous studies in which unknown mechanism was uncovered by observational studies in the field of hippocampus- and amygdala-dependent memory [22, 34, 35], observational studies would make a significant contribution to discovering unknown molecules or mechanisms related to motor memory.

In this dissertation, I conducted observational studies to suggest possible molecular and cellular traces for cerebellum-dependent motor memory. To do this, I used the adaptive behavior in the oculomotor system as a behavioral paradigm, which is well known as a simple paradigm for cerebellum-dependent motor learning and memory [36]. The following two studies were performed using the cerebellum

obtained from mice that were learned by oculomotor adaptation.

In chapter I, I performed a mass-spectrometry-based quantitative proteomic analysis to identify candidates of traces for cerebellum-dependent motor memory at the molecular level. Although de novo protein expression is essential to form memory [7], proteomic profiling has not yet been attempted in the field of cerebellum-dependent motor memory. In this study, I used three different oculomotor learning paradigms and quantified the proteins in the cerebellum prepared in each learning paradigm. Statistical and advanced bioinformatic analyses were applied to discover distinct protein networks in the three learning paradigms.

In chapter II, I evaluated the electrophysiological properties in the cerebellar Purkinje cells taken from mice that underwent cerebellum-dependent motor learning. Even though the cerebellar Purkinje cells, the sole output of the cerebellar cortex, have been well studied for synaptic plasticity and intrinsic excitability [37, 38], a few observational approaches related to electrophysiological properties have been made in the field of cerebellum-dependent motor memory. In this study, fresh cerebellar slices were prepared from animals that experienced oculomotor learning, and then the whole-cell patch-clamp recording technique was used in the cerebellar Purkinje cells to compare the intrinsic and synaptic excitabilities with the results from the control group.

Chapter I. Quantitative Proteomics Reveals Distinct Molecular Signatures of Different Cerebellum-Dependent Learning Paradigms

INTRODUCTION

Cerebellum-dependent motor learning is the process of improving the accuracy of motor performance by adjusting movement gain (e.g., increasing or decreasing the gain of movements). An early hypothesis proposed that the adaptive changes in desired motor output are accomplished by modification of the efficacy of certain synapses in the cerebellar cortex [39-41]. The studies using oculomotor adaptation, one of the most studied cerebellum-dependent motor learning paradigms, have been consistently demonstrating the relationship between the synaptic plasticity at certain synapses in cerebellum and motor gain [42-51]. However, accumulating evidence indicates that the changes in synaptic efficacy at certain synapses in the cerebellar cortex cannot solely account for the direction-selective motor learning by the cerebellum [24, 25, 37, 52-54]. At the behavioral level, increases and decreases in oculomotor gain possess different learning kinetics and reverse each other with unequal efficacy, which suggests the direction-selective motor learning is implemented by different plasticity mechanisms [55]. Moreover, genetic or pharmacological manipulation in animals to modulate the activity of molecules associated with synaptic plasticity in cerebellar synapses have reported 1) selective or prominent deficits in a specific direction of oculomotor learning [47, 48, 54, 56, 57], 2) broad effects on oculomotor learning regardless of the direction [43, 58-61], or 3) no effect on oculomotor learning [62].

As mentioned above, the cerebellum occupies an important position in the direction-selective motor learning, but the underlying cellular mechanism may vary depending on the learning direction. The fundamental nature of memory storage in the brain lies in the ability to alter functional or structural synaptic connectivity, for which *de novo* protein synthesis is critical [4]. Hence, I hypothesized that oppositely directed motor learning would induce distinct patterns of protein expression in the cerebellum over the time course of memory retention after learning. To test my hypothesis, I used a mass-spectrometry-based quantitative proteomics technique combined with a simple animal model of cerebellum-dependent motor learning. Modern proteomics technology has been successfully used in researching the

widespread network changes of proteomes and the identification of previously unknown molecules [63, 64]. As an animal model of direction-selective motor learning, I used the oculomotor system, such as the vestibulo-ocular reflex (VOR) and optokinetic response (OKR). The VOR is a compensatory eye movement evoked by the motion of head in an opposite direction to the head movement to stabilize an image on the retina. The OKR is a reflexive eye movement driven by the motion of visual field. Both reflexes are known to show adaptive changes in motor gain, which is dependent on the cerebellum [36]. I recruited a bidirectional learning paradigm of these reflexes that can increase (VOR-up and OKR-up) or decrease (VOR-dn) the gain of the reflex, with combinations of visual and vestibular stimulation.

Oculomotor memory is known for its time-dependent characteristics over the time course of memory consolidation [65, 66]. In the current study, I quantified proteins in the cerebellum at 24 h after the learning. In general, it is well-known that protein expression at this time-point is important for memory retention in various regions of the brain [4]. Recent studies have also suggested that unknown mechanisms may be engaged in the retention of oculomotor memory at that time [67, 68]. Besides, since a list of cerebellar proteins involved in the initial period of motor memory formation also remains unknown, samples obtained at 1 hr after the training were added to my proteomic quantification. In this regard, I expected to identify regulated proteins not only at the critical period but also at the early phase of memory formation.

In this study, I conducted proteomic profiling with samples taken at 1 and 24 hrs after learning from mice that had undergone three different oculomotor learning paradigms. Statistical analysis of quantitative proteomics was applied to identify significantly regulated proteins and protein sets that may be involved in the molecular mechanisms of distinct forms of cerebellar learning at 1 and 24 hrs after learning, respectively. In-depth bioinformatic analysis identified a comprehensive list of molecules that were highly correlated with behavioral outcomes. Furthermore, four proteins out of five selected proteins were validated by a different experimental method such as western blot. My findings provide new insight into the molecular pathways underlying bidirectional cerebellum-dependent motor learning.

MATERIALS AND METHODS

Animals

Male C57BL6/J mice (Central Lab. Animal Inc., KOREA) aged 7-12 weeks old were used. Animals were housed with food and water available *ad libitum* under a 12 h light/dark cycle except during consolidation sessions for oculomotor memory, which animals were housed in complete darkness. Experimental procedures were approved by the Animal Care and Use Committee of Seoul National University.

Behavioral tests

Surgical procedure. The whole surgical process was done under isoflurane anesthesia. In order to restrain the mouse's head during the behavioral test, a headpost was mounted with two M2 nuts, four screws (M1.2 x 5.5), and dental cement (Super bond C&B, Sun Medical, Japan). Nuts were placed approximately on the lambda and bregma of the skull, and screws were implanted beside the nuts. Finally, dental cement was applied between the nuts and screws following the manufacturer's instruction. Mice were given for at least 24 hours after surgery.

Preparation for behavioral procedure. For two days of acclimation, animals were restrained with a custom-made restrainer 15 min both with and without light for habituation to the recording environment. Calibration was performed according to the procedure reported by Stahl et al. (2000) [69]. The recorded stimulus (movement of the screen or turn-table) and response (evoked eye movement) were smoothed and fitted to sine curves. I obtained the gain, a ratio of the eye response to the visual or vestibular stimulus, respectively, for the OKR or VOR.

Learning protocols. Behavioral sessions consisted of training and consolidation sessions. The training session contained five 10-min training blocks and six check-points. After the training session, mice were kept in complete darkness for 1 or 24 h to form short-term memory (STM) or long-term memory (LTM), respectively. Then, the final OKR or VOR was measured before brain sampling. I recruited a control (Ctrl) and oculomotor trained group. The trained group was further divided into three groups with a combination of the OKR and VOR protocol. For Ctrl and OKR-up groups, OKR was measured in response to sinusoidal oscillation of the screen with

an amplitude of 5° and frequency of 0.5 Hz before and after the training session. During the training session, the OKR-up group was subjected to the repeated oscillation of the screen with an amplitude of 5° and frequency of 0.5 Hz, while the Ctrl group experienced an identical environment to that of the OKR-up group with the exception of visual stimulation (Figure 1.2A). For the VOR-up and VOR-dn groups, VOR was measured in response to sinusoidal movement of the turn-table with 0.5 Hz frequency and ± 5° amplitude before and after the training session under light-off conditions. Visual stimuli in the same direction as that of vestibular stimuli induced a decrease of VOR in the VOR-dn group (Figure 1.2C, bottom left), whereas visual stimuli in the opposite direction to that of vestibular stimuli induced an increase of VOR in the VOR-up group (Figure 1.2C, top left). A linear mixed model post-hoc Tukey test was used to examine changes in oculomotor gain over time within a group.

TMT-labeled mass-spectrometry

All TMT-labeled mass-spectrometry procedures, including sample preparation, data processing, searching, quantification, and normalization were performed in collaboration with Proteomics & Biomarker Laboratory at Seoul National University College of Medicine (Professor Youngsoo Kim). Detailed materials and methods can be found in the article published in the Journal of Proteome Research [70].

Bioinformatics

Gene ontology (GO) analysis. GO analysis was performed using the Database for Annotation, Visualization and Integrated Discovery (DAVID) Bioinformatic Resource (http://david.ncifcrf.gov/home.jsp) [71]. In GO analysis, three GO domains, biological process (BP), cellular component (CC), and molecular function (MF), were used. GO analysis was used to annotate the biological function of DEPs in the quantitative proteomic analysis (Table 2), and of proteins in the significant modules in WGCNA (Figure 1.6). The significance level was set to FDR < 0.25. Given that my study is the first attempt to address the molecular nature of cerebellum-dependent memory using proteomic profiling, I used a less stringent FDR cutoff to yield more candidate pathways which shall be validated in further research. For this purpose, several studies utilized this criterion [72].

Protein set enrichment analysis (PSEA). Protein set enrichment analysis (PSEA)

was run by desktop application with gene sets of Gene Ontology Biological Process (GO BP) v6.1 downloaded from the web (software.broadinstitute.org/gsea/downloads.jsp) [73]. In PSEA, I compared to control (n=3) with three trained groups: OKR-up, VOR-up, and VOR-dn (n=3 per group), respectively. Small (less than 15 genes) or large (more than 500 genes) gene sets were discarded from the analysis. The primary result of the PSEA was the enrichment score, which reflected the degree to which a protein set was overrepresented at the top or bottom of a ranked list of proteins. The enrichment score of each protein set was normalized considering the size of the protein set to yield a normalized enrichment score. PSEA results were filtered using the criteria of FDR < 0.25 to perform enrichment clustering analysis.

Enrichment clustering analysis. Enrichment Map is a network-based clustering tool for PSEA results [74]. Free software is available on the web (http://www.baderlab.org/Software/EnrichmentMap). The tool clusters similar gene sets based on the overlap coefficients, which depend on the number of shared genes in the gene sets. In my results, protein sets were clustered if their overlap coefficient was > 0.4 (i.e., protein sets sharing 40% or more proteins). Protein set clusters having less than three protein sets (edges) were removed from the results. Clustered protein set lists and results of PSEA are available in Supplemental Table S3. I generated a heatmap using FDR values of clustered protein sets, which were extracted from PSEA results (Figure 1.5C). Both colors indicate FDR values, while blue and red indicate that the protein expression of the significant protein sets in the trained group was down-regulated and up-regulated compared to those in the control group, respectively.

Protein co-expression network analysis. Weighted protein co-expression network analysis was conducted using the freely accessible R package WGCNA (weighted gene co-expression network analysis) [75]. In detail, before the analysis, I separated the whole profiling of the LTM group results into two data-sets based on the oculomotor class. 24H-Ctrl and 24H-OKR-up were classified as the OKR-set. 24H-VOR-up and 24H-VOR-dn groups were grouped into the VOR-set. In each data-set, a pair-wise Pearson correlation (r) matrix was created for all detected proteins to calculate the coexpression similarity. Next, the scale-free topological overlap metric,

a signed weighted adjacency matrix, was derived from the correlation matrix by applying the approximate scale-free topology criterion with a soft power threshold of 26. The resulting adjacency matrix was then used for calculation of the topological overlap matrix (TOM) to identify modules of highly coexpressed proteins. A cluster dendrogram, generated by hierarchical clustering of proteins on the basis of their topological overlap, was cut into modules of minimal size using a Dynamic Tree Cut algorithm with a height of 0.25, and a minimum module size of 50. To characterize the modules and the relationship between them, I calculated the first principal component (module eigenprotein; ME) for each module. ME corresponded to a theoretical ideal representative protein member among all proteins in a given module. Based on the protein co-expression modules, WGCNA identified modules that were significantly associated with behavioral traits. A trait-based Protein Significance (PS) represented the absolute correlation between the traits and protein expression profiles. Module Membership (MM) was the correlation between each the ME and protein expression profile. I selected four oculomotor observations, Post Gain, STM Gain, LTM Gain, and ΔGain, as behavioral traits. Post Gain is the gain after the training session (+50 min). STM Gain and LTM Gain refer to the gain at 1 and 24 hrs after the training session, respectively. In addition, I calculated ΔGain by subtracting gain at 0 min in the training session from the final gain (at 1 hr or 24 hrs after the training session). In an intramodular analysis of WGCNA, a p-value was obtained from a linear regression model between the eigenprotein and the trait to test statistical significance between the module eigenprotein and the trait. Significance level of the relationship between each module and the behavioral trait was set to p-value ≤ 0.01.

Biological validation

Behavioral tests and sampling. For biological validation of proteomic profiling results, independent biological samples were prepared. In addition to Ctrl and OKR-up groups in the same way as proteomic profiling, I added a home-cage control (Home-Ctrl) group to the experimental control group. Home-Ctrl group was kept in the home-cage without any preparation or procedures for the behavioral tests, then sacrificed to extract proteins from the cerebellum. The OKR training session was 300 cycles of 2-sec optokinetic stimulations (10 min). The OKR-up group was

subjected to five training sessions. The OKR was measured before and after each session. For the Ctrl group, OKR was measured at the same intervals as those of the OKR-up group without training sessions. Both Ctrl and OKR-up groups were kept in complete darkness for 24 h. Cerebella of both groups were collected after the final measurement of OKR.

Western blot analysis. After the samples were lysed with lysis buffer (4% SDS, 0.1 M Tris-Cl, 1 mM TCEP) and heated at 98°C for 30 minutes, the same amount (15 μg) of protein was loaded per lane of 4-8% Bis-Tris polyacrylamide gels. Following electrophoresis, the proteins were transferred to a PVDF membrane. The membranes were washed five times with TBS-T (Tris-buffered saline and Tween 20) for 1 hour followed by incubation with horseradish peroxidase-conjugated secondary antibodies for 2 hours at room temperature. After being washed with TBS-T for 1 hour, the membranes were developed with a mixture of detection solution (West-Q Chemiluminescent Substrate Kit-plus, GenDEPOT, Barker, TX, USA) and quantified on an image reader (LAS-4000, Fujifilm, Japan). The resulting western blot images were scanned using LAS-4000 mini software (Fujifilm, Japan). One-way ANOVA with Bonferroni's post-hoc test was used for comparison among Home-Ctrl, Ctrl, and OKR-up groups. The level of significance was set at p-value ≤ 0.05. Primary antibodies for Snca (α-synuclein, #ab1903), Sncb (β-synuclein, #ab76111), Cplx2 (Complexin2, #ab215046), and Stmn1 (Stathmin1, #ab52630) were purchased from Abcam (Cambridge, UK). Antibodies for Cttn (Cortactin, #sc-55579) and Actb (Beta-actin, #sc-47778) were obtained from Santa Cruz Biotechnology (Dallas, TX, USA). Secondary antibodies for goat anti-rabbit HRP (#ab6721) and goat anti-mouse HRP (#ab6789) were obtained from Abcam (Cambridge, UK). Antibody for rabbit anti-sheep HRP (#31480) was purchased from Thermo Scientific (Rockford, IL, USA).

Real-time quantitative PCR. Expression level of transcripts of target proteins was quantified in Home-Ctrl (n=3) and LTM of OKR-up (n=3) groups by real-time (RT) quantitative PCR (qPCR). Cerebellar flocculi were obtained from 7-12 weeks old mice (n=3). Total RNA was purified from the collected sample using the RNeasy Mini Kit (QIAGEN) according to the manufacturer's instructions. Isolated total RNA was quantified by Nanodrop (ThermoFisher). The same amount of total RNA

per sample was reverse transcribed into cDNA using SuperScript III First-Strand (Invitrogen). RT qPCR was conducted using the CFX Connect system (Bio-Rad) with primers selected from the Harvard Primer Bank (http://pda.mgh.harvard.edu/primerbank/index.html). Primer sequences are available upon request. Mean Ct values were used relative quantification of mRNA expression between Home-Ctrl and OKR-up group using the Pfaffl's (2001) method [76], with the ratio of the target gene expressed relative to the mean of Actb (β-actin).

RESULTS

The schematic workflow of my study is shown in Figure 1.1. First, behavioral experiments were conducted using mice to prepare a cerebellum-dependent motor learning model. After the end of the behavioral experiment, the cerebelli collected from each animal were subjected to TMT-labeled mass spectrometry to quantify protein expression in each sample. Differential expression analysis and GO analysis were performed for both STM and LTM groups. In addition, in-depth bioinformatic analysis was performed on the LTM group.

Induction of three oculomotor memories in mice

To reveal distinct changes in protein expression induced by different forms of oculomotor learning, C57Bl/6 mice were subjected to three different training paradigms: OKR-up, VOR-up, or VOR-dn. Exposure of mice to continuous visual stimuli without vestibular stimulation led to an increase of the OKR (OKR-up, Figure 1.2A bottom). Rotating the screen in the opposite direction to the head adaptively increased the gain of the VOR (VOR-up; Figure 1.2C, top), while rotating the screen in the same direction as the head decreased the gain of the VOR (VOR-dn; Figure 1.2C, bottom). As a control, I used mice that were subjected to identical conditions to those of the OKR-up group with the exception of visual stimulation (Ctrl; Figure 1.2A, top).

I trained mice using OKR-up, VOR-up, and VOR-dn learning paradigms. In contrast to the Ctrl group, which did not receive either visual or vestibular stimulation, the OKR-up group was trained under continuous oscillation of the screen for 50 min. OKR gain in the Ctrl group did not exhibit significant change during the training session ($F_{(5)}$=1.98, p=0.12, linear mixed model). Conversely, OKR gain in the OKR-up group significantly increased after learning ($F_{(5)}$=27.62, p < 0.0001, a linear mixed model with post-hoc Tukey test) (Figure 1.2B). Acquired memory in the OKR-up group was successfully maintained until +24 h after training ($F_{(2)}$=9.7E-4, p=0.99, linear mixed model) (Figure 1.2B). I induced VOR-up and VOR-dn learning in mice by pairing the head rotation with rotation of the screen. Brief training of VOR-up and VOR-dn induced significant changes in VOR gain (Figure 1.2D) (VOR-dn: $F_{(5)}$=32.47, p < 0.0001, VOR-up: $F_{(5)}$=15.6, p < 0.0001,

linear mixed model). The amount of learning was fully retained during the consolidation session similar to previous reports (Figure 1.2D) (VOR-dn, $F_{(2)}$=3.22, p=0.0831; VOR-up, $F_{(2)}$=2.41, p=0.14, linear mixed model) [42, 55, 67]. After confirming that the mice had learned each task either at 1 or 24 h after learning, brain tissue was collected for proteomic analysis.

Quantitative proteomic analysis

Next, I performed quantitative proteomic analyses using isobaric labeled tagging to test whether protein expression in the cerebellum differs among animal groups depending on the oculomotor learning paradigm and consolidation time. I carefully dissected cerebellar flocculi, which is an essential subregion of the cerebellum for OKR and VOR learning [41]. In 36 LC-MS runs with 2,287,373 MS/MS spectra, 58,892 peptide sequences were identified with an FDR < 0.01, matching to 6,623 protein groups (Figure 1.3A). Relative quantification of 5,347 protein groups was enabled by utilizing the criteria of three valid values in at least one group. Out of the total quantified proteins, 84% of the proteins had a valid value in all 24 samples, and 12% of the quantified proteins had 65% valid values in the 24 samples. About 4% of the proteins had a 65% missing value. Quantitative analysis was performed by substituting the missing values with the imputation algorithm in Perseus software (Supplemental Table S2 at https://pubs.acs.org/doi/10.1021/acs.jproteome.9b00826). The FASP digestion for protein and high-pH reverse phase fractionation techniques for peptides used in this study contributed to the discovery of 22.2% of membrane proteins, 19.8% of cytoplasmic proteins, and 15.3% of nuclear proteins (Figure 1.3B). Quantile normalization corrected for global linear experimental variation as long as the abundance ranks of the proteins remained similar between samples. Although quantile normalization made the distribution of ratio values nearly identical between the samples, it was inappropriate to combine data sets without adjusting for batch effects. introduced two total samples (channel at 128C and 131) per TMT set in order to check the differences between the experimental sets and deviation between channels. I confirmed that the effects of the batch that appeared to change the ranking of important proteins still existed (R<0.93, Figure 1.3C). The present study recruited a large-scale analysis technique using multiple samples, which required a standardization method to eliminate non-biological diversity. Adjustment of batch

effects is crucial for statistical models that do not include batch factors because quantile normalization does not change the level of proteins. Eliminating non-biological changes could have lowered the p-value in statistical tests and I adjusted the threshold accordingly. Using the Combat algorithm, I confirmed that batch effects were adequately removed by measuring the correlation between each pooled sample (R=1.00, Figure 1.3C).

Comparing proteins identified in cerebellar flocculi of control and trained groups, I identified 21and 22 DEPs that met the threshold greater than 1.2-fold change or less than 0.8-fold change in expression with a p-value $\leq$ 0.05 in STM and LTM groups, respectively (Table 1). The number of DEPs was the largest in 24H-OKR-up (17 proteins), followed by 01H-VOR-dn (11 proteins) and 01H-OKR-up (9 proteins) (Figure 1.4). I performed GO analysis using DAVID to annotate the biological functions of these regulated proteins (Table 2). GO analysis using CC domain revealed that 23 of the 43 regulated proteins were cytosolic proteins and many of them were known to localize and be active at dendrite, synapse, or neuronal cell body.

Table 1. The significantly upregulated and downregulated proteins in cerebellar flocculus after oculomotor learning

#	Accession	Gene name	Folds (Trained/Control)	P-value	Learning paradigm	
1	Q78J03	Msrb2	1.206	0.008	VOR-dn	
2	Q8BXC6	Commd2	1.283	0.018	VOR-dn	
3	Q8BX80	Engase	1.236	0.047	VOR-dn	
4	P11881-6	Itpr1	1.235	0.011	VOR-dn	
5	F7BNZ5	Bcas1	1.204	0.013	VOR-dn	
6	Q925N1	Sfxn4	1.215	0.029	VOR-dn	
7	Q69ZS6	Sv2c	1.237	0.024	VOR-dn	
8	Q8C7M3	Trim9	0.798 / 0.795	0.032 / 0.030	VOR-dn / VOR-up	
9	Q9CZJ2	Hspa12b	0.771	0.028	VOR-dn	
10	E9PWI3	Mcc	0.775 / 0.748	0.006 / 0.005	VOR-dn / OKR-up	01 H
11	Q64332-2	Syn2	0.728	0.040	VOR-dn	
12	Q3U2V3	Nudt18	1.212	0.040	VOR-up	
13	Q61033	Tmpo	0.769 / 0.800	0.012 / 0.022	VOR-up / OKR-up	
14	Q9ERE8	Mesdc1	0.728	0.029	VOR-up	
15	A2BDX0	Adnp	1.289	0.027	OKR-up	
16	Q8CCS2	Fam155a	1.322	0.008	OKR-up	
17	Q3UYK2	Psen1	1.338	0.034	OKR-up	
18	Q6P9J5	Kank4	0.786	0.021	OKR-up	

19	P28481	Col2a1	0.781	0.016	OKR-up	
20	Q9D8S9	Bola1	0.694	0.020	OKR-up	
21	Q64362	Aktip	0.768	0.002	OKR-up	
22	Q3UV17	Krt76	1.402	0.046	VOR-dn	
23	B6ZHD1	Epb41l3	1.262	0.034	VOR-dn	
24	Q8BP27	Sfr1	1.303	0.005	VOR-up	
25	P28653	Bgn	0.779	0.022	VOR-up	
26	P07309	Ttr	0.790	0.026	VOR-up	
27	P84086	Cplx2	1.242	0.031	OKR-up	
28	E9PUC5	Psd3	1.422	0.015	OKR-up	
29	F8WHQ1	Tpd52	1.212	0.013	OKR-up	
30	Q9CPX6	Atg3	1.233	0.043	OKR-up	
31	Q3UIL6-2	Plekha7	1.329	0.013	OKR-up	
32	Q60598	Cttn	1.211	0.009	OKR-up	24 H
33	Q8K2K6	Agfg1	1.218	0.028	OKR-up	
34	Q545B6	Stmn1	1.222	0.014	OKR-up	
35	A8IK50	Pcp2	1.261	0.025	OKR-up	
36	Q91ZZ3	Sncb	1.402	0.021	OKR-up	
37	O55042	Snca	1.237	0.032	OKR-up	
38	D3Z4V2	Fip1l1	1.385	0.003	OKR-up	
39	Q3UMC8	Stam	1.234	0.025	OKR-up	
40	Q68FM7	Arhgef11	0.763	0.014	OKR-up	
41	Q9DCU2	Pllp	0.791	0.037	OKR-up	
42	Q8C622	Hist1h2bp	0.727	0.040	OKR-up	
43	Q8BVR6	Rspry1	0.799	0.018	OKR-up	

Table 2. Oculomotor learning-regulated proteins implicated in the synaptic function.

Functional annotation	p-value	# of proteins	Proteins
Cell junction	6.85E-05	9	Epb41l3, Cttn, Psen1, Plekha7, Trim9, Syn2, Snca, Psd3, Sv2c
Synapse	4.42E-04	7	Cplx2, Sncb, Trim9, Syn2, Snca, Psd3, Sv2c
Neuronal cell body	5.94E-04	7	Cplx2, Agfg1, Sncb, Psen1, Pcp2, Adnp, Itpr1
Postsynaptic density	1.25E-03	5	Epb41l3, Bcas1, Syn2, Psd3, Itpr1
Terminal bouton	1.45E-03	4	Cplx2, Sncb, Syn2, Snca
Synaptic vesicle	1.98E-03	4	Trim9, Syn2, Snca, Sv2c
Cytoplasm	2.98E-03	23	Bcas1, Cplx2, Sncb, Snca, Adnp, Col2a1, Tpd52, Engase, Atg3, Kank4, Itpr1, Arhgef11, Epb41l3, Hist1h2bp, Cttn, Bgn, Aktip, Trim9, Plekha7, Commd2, Stam, Mcc, Stmn1
Growth cone	3.83E-03	4	Cttn, Sncb, Psen1, Snca
Dendrite	1.57E-02	5	Cplx2, Psen1, Trim9, Adnp, Itpr1

Identification of distinct patterns of protein expression in LTM group

As a result of the differential expression analysis, I summarized a list of proteins that were differentially regulated in the cerebellum of three oculomotor trained mice at 1 and 24 hrs after the training (Figure 1.4 and Table 1). However, the number of DEPs limited further analysis beyond the GO assay. To overcome this limitation, I applied a bioinformatic approach known as Gene Set Enrichment Analysis (GSEA) to my quantitative proteomics data of LTM group. GSEA is a threshold-free approach that analyzes all genes on the basis of their differential expression rank without prior gene filtering [73]. GSEA was originally developed for gene expression analysis using microarrays but there have been attempts to apply the GSEA theory to proteomics data [77].

I performed Protein Set Enrichment Analysis (PSEA) using GO BP v6.1 as an *a priori* defined protein set. PSEA results showed that the number of significant protein sets (FDR < 0.25) was close to or exceeded 100 in LTM group (24H-VOR-dn, 119; 24H-VOR-up, 96; 24H-OKR-up, 103 protein sets) (Figure 1.5A). In PSEA results of each trained group, I examined whether protein expression in these significant protein sets was up-regulated (negative enrichment score) or down-regulated (positive enrichment score) compared to those of the control group. In 24H-VOR-dn and 24H-VOR-up groups, the expression of most significant protein sets was down-regulated compared to those of the Ctrl group, whereas most of the protein sets were up-regulated in 24H-OKR-up groups (Figure 1.5A). The normalized enrichment score of the top three protein sets in PSEA results for each learning paradigms of LTM is shown in Figure 1.5B.

In the PSEA, I used GO BP v6.1 containing 4436 gene sets. This large gene-set collection made the list of results longer and increased the redundancy between sets, making interpretation of results more challenging. Thus, I clustered PSEA results based on overlap coefficients using Enrichment Map, a network-based clustering tool for GSEA [74] (see Materials and Methods). Clustering analysis of the significantly regulated protein sets returned 11 clusters (Figure 1.5C). The set of proteins belonging to 'Cell, Matrix adhesion' and 'Cell substrate adhesion' function was significantly modulated in the 24H-VOR-dn group (cluster 1 and 2). Cluster 3 (Cellular response to acid) and 4 (Organic acid transport) were selectively regulated

in 24H-VOR-up group. Cluster 5 (Extracellular matrix structure), 6 (Granule, Exocytosis), 7 (Organ, morphogenesis), and 8 (Brain development) were commonly regulated in both of 24H-VOR-dn and -up groups. In contrast, protein sets coding for 'Regulation of cytoskeleton' (Cluster 9), 'Neurotransmission' (Cluster 10), and 'Ca^{2+} channel, Cation transport' (Cluster 11) were highly regulated in the 24H-OKR-up group, but not in other trained groups.

Discovery of signature proteins correlated with oculomotor memory using co-expression network analysis

As I collected all the samples after behavioral tests, I searched for a group of proteins whose expression was significantly correlated with oculomotor memory using weighted gene co-expression network analysis (WGCNA), a popular bioinformatics method that analyzes complex relationships between genes and external traits [75]. I divided my proteomics data into two sets based on two oculomotor classes, OKR and VOR, then conducted WGCNA (see Materials and Methods). OKR-set was composed of control and 24H-OKR-up groups. 24H-VOR-up and 24H-VOR-dn groups were paired into VOR-set. I selected Post Gain, STM Gain, LTM Gain, and ΔGain as behavioral traits for WGCNA. Post Gain was the gain after the training session (+50 min). STM Gain and LTM Gain referred to the gain at 1 and 24 h after the training session, respectively. ΔGain represented the difference between the pre-training and final gain.

WGCNA of the OKR-set produced 36 distinct modules, each containing similarly expressed proteins. Of 36 modules, seven modules were significantly correlated with any of four behavioral traits (p < 0.05) (Figure 1.6A). Of the four traits I measured, Post_Gain, STM_Gain, and LTM_Gain denoted the absolute values of the oculomotor performance measured at each time, while ΔGain was derived by subtracting the pre-training performance from the post-training performance of each animal (see Materials and Methods). Therefore, I considered ΔGain to be a more precise measure representing the amount of learning in each animal. For the intramodular analysis in WGCNA, I used ΔGain as a trait of interest, and identified modules that were significantly associated with learning amount.

Module18 (192 proteins) demonstrated a negative correlation with ΔGain in OKR-up learning (r = -0.97, p = 2e-03) (Figure 1.6B). Module32 (486 proteins) was

positively correlated with ΔGain (r = 0.95, p = 3e-03) (Figure 1.6C). To facilitate biological interpretation for these two modules, functional annotation of the proteins in each module was performed using DAVID with GO terms. Functional annotation analysis showed that proteins in Module18 were significantly enriched in GO BP term of "transport" (Fold enrichment 1.92, 34 proteins), CC term of "mitochondrion" (fold-enrichment 2.55, 42 proteins), and MF term of "hydrolase activity" (fold-enrichment 2.19, 32 proteins) (Figure 1.6D). Proteins in Module32 were significantly enriched in GO BP term of "cell-cell adhesion" (fold-enrichment 5.51, 26 proteins), CC term of "cytoplasm" (fold-enrichment 1.78, 227 proteins), and MF term of "cadherin binding involved in cell-cell adhesion" (fold-enrichment 5.53, 38 proteins) (Figure 1.6E). Regarding the VOR-set, only one module (Module25) was significantly correlated with Post Gain, and none had a significant correlation with the ΔGain (Figure 1.7). The top five of GO BP, CC, and MF terms enriched in Module18 and Module32 are shown in Figure 1.6D and E, respectively. All WGCNA results including functional annotation of the significant modules are available in Supplemental Table S4 at https://pubs.acs.org/doi/10.1021/acs.jproteome.9b00826.

Biological validation of selected proteins

To validate the expression profile in independent biological samples using a different experimental method such as western blot, I used the results of WGCNA to select target-proteins for biological validation. Module32 from WGCNA was positively correlated with the learning amount in the OKR-set (Figure 1.6). Of 486 proteins in Module32, ten proteins satisfied the condition of 1.2-fold change or higher in the 24H-OKR-up (Figure 1.8). I selected five of ten proteins, Snca (α-Synuclein), Sncb (β-Synuclein), Cttn (Cortactin), Stmn1 (Stathmin1), and Cplx2 (Complexin2), for biological validation.

First, animals were prepared to obtain an independent set of samples. Ctrl (n=8 mice) and OKR-up (n=8 mice) groups were prepared in the same way as those for proteomic profiling analysis. The home-caged control group (Home-Ctrl, n=5 mice) was newly recruited. Mice in the Home-Ctrl group were housed only in their home-cage before brain sampling for protein extraction. In the behavioral test, I reconfirmed that gain in the OKR-up group rapidly increased over training sessions compared to gain in the Ctrl group, and learning amount in the OKR-up group was

retained well after 24 hours (Ctrl, $F_{(6)}$=3.25, p=0.01; OKR-up, $F_{(6)}$=48.89, p<0.0001, linear mixed model) (Figure 1.9A). Five pairs of cerebellar flocculus per group were subjected to western blot analyses.

Of the five selected proteins, the expression level of four proteins (Snca, Sncb, Cttn, Stmn1) exhibited a similar pattern to that of the proteomic quantitation level except for Cplx2 (Figure 1.9B). Protein expression was significantly increased in the OKR-up group compared to that in the Home-Ctrl group (Snca, p<0.001; Sncb, p<0.001; Stmn1, p<0.001, one-way ANOVA with post-hoc Bonferroni test). Furthermore, I examined the transcript level of the five selected by performing real-time quantitative PCR analysis (Supplemental Methods). I observed that the mRNA expression of four upregulated proteins was increased in the OKR-up group (3 mice) compared to the Home-Ctrl group (3 mice) (Figure 1.10).

Since the target proteins were extracted from the highly correlated module with the learning amount of OKR-up learning in WGCNA, correlation analysis performed between the protein expression measured by western blot and ΔGain of OKR-up learning. Correlation analysis including both Ctrl and OKR-up groups (n=5 mice per group) revealed a strong positive correlation (r > 0.6) between protein expression and ΔGain of OKR-up learning in Snca (Figure 1.9C, r=0.75, p=0.012), Sncb (Figure 1.9D, r=0.86, p=0.0015), and Cttn (Figure 1.9E, r=0.64, p=0.048).

Finally, western blot analysis of four confirmed proteins was conducted using a new set of samples obtained from VOR-dn (n=3) and VOR-up (n=4) paradigms to confirm whether these proteins were selectively increased in the OKR-up paradigm (Figure 1.11A). As expected from the results of proteomic profiling, large increases seen in the OKR-up group were not observed in the VOR-up and VOR-dn groups (Figure 1.11B and C), supporting the fidelity of my proteomic analyses.
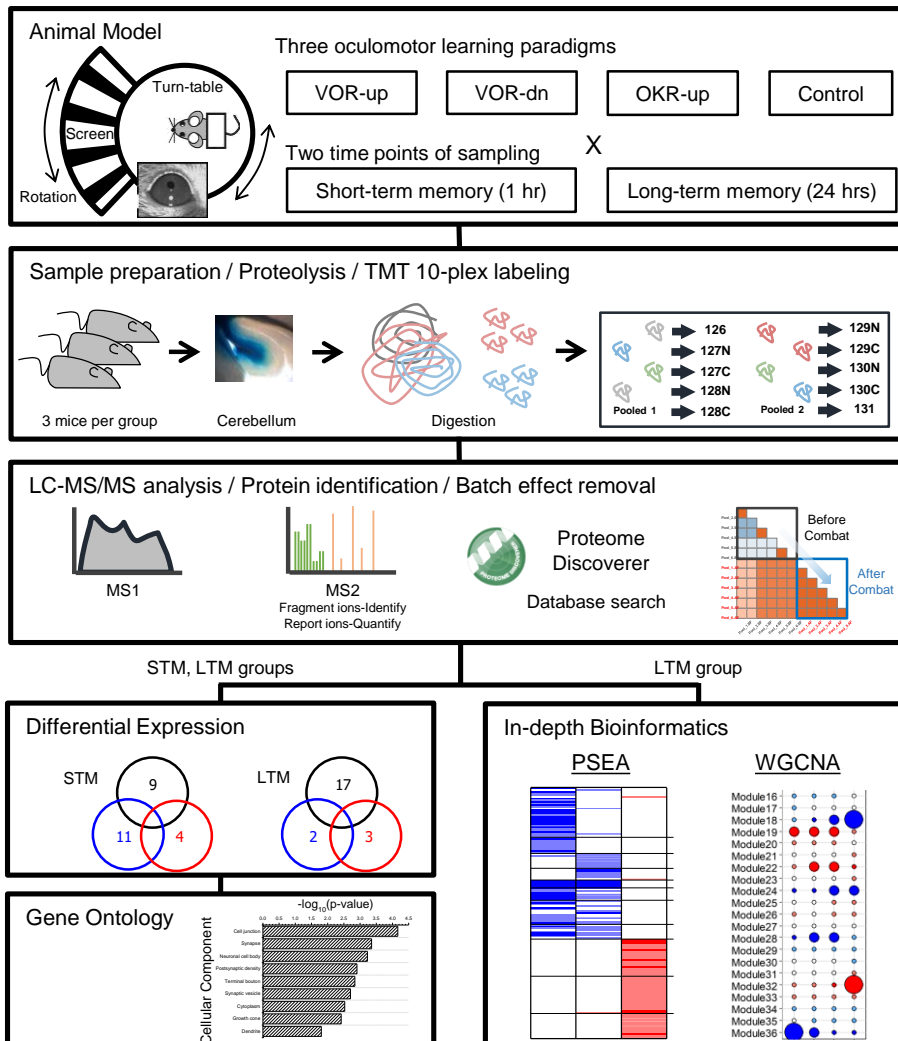
Figure 1.1. Workflow of the present study. The TMT-labeled quantitative proteomics was performed with eight groups of mice (three oculomotor learning and one control groups with two time points) (3 mice per each group). For both short-term memory (STM) and long-term memory (LTM) groups, differential expression and gene ontology analyses were utilized to discover a list of DEPs and their biological functions. In-depth bioinformatic analysis, such as protein-set enrichment analysis (PSEA) and weighted gene co-expression network analysis (WGCNA), were subjected to LTM group only to reveal distinct expression patterns of the protein network for each learning paradigm. The whole TMT-labeled quantitative proteomics, including proteolysis, LC-MS/MS analysis, and protein identification, was performed in collaboration with Proteomics & Biomarker Lab at Seoul National University (Professor Youngsoo Kim).
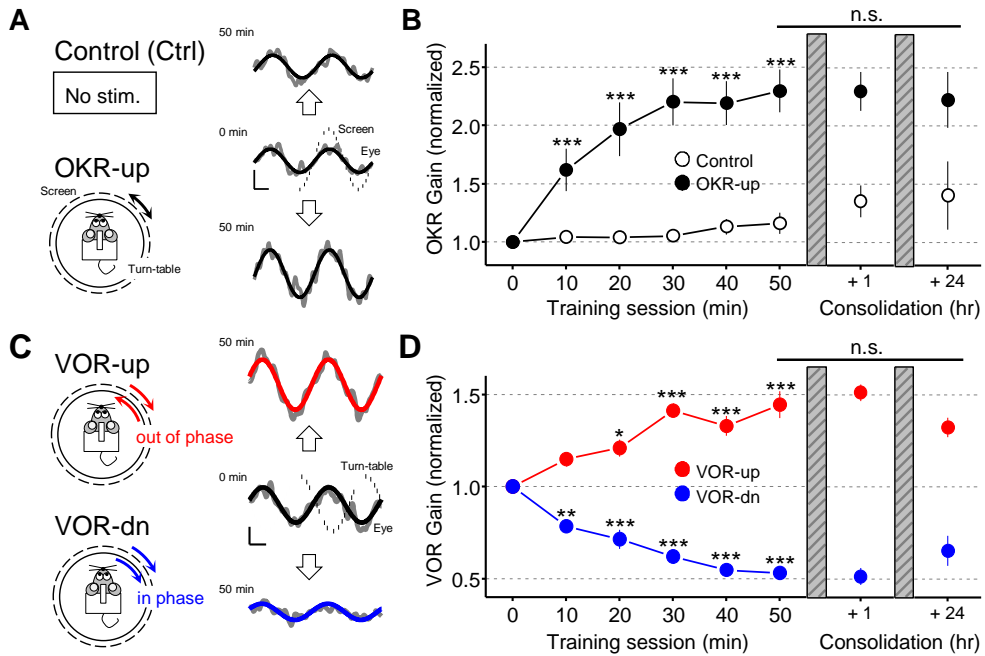
Figure 1.2. Three cerebellum-dependent oculomotor learning in mice. (A) Control (Ctrl) and OKR-up groups. In contrast to the Ctrl without visual stimulation, OKR-up group experienced continuous oscillation of the screen (dashed circle) with an amplitude of 5 deg at 0.5 Hz for 50 min (left bottom). Representative eye (gray: raw, black: curve-fitted) and the screen (dashed) traces recorded before (0 min) and after (50 min) the training are shown in the right panel. (B) Changes in OKR gain of Ctrl (n=8, white circle) and OKR-up (n=8, black circle) group during training and consolidation. (C) VOR-dn and VOR-up groups. For VOR-up group, the screen and the turn-table (black circle) oscillated in opposite directions (red arrows) (left top). For VOR-dn group, the screen and turn-table moved sinusoidally in the same directions (blue arrows) with an amplitude of 5 deg at 0.5 Hz (left top). Decreased VOR gain after VOR-dn learning (blue trace) and increased VOR gain after VOR-up learning (red trace) are depicted in the right panel. In this panel, the dashed line represents traces of the turn-table. (D) Changes in VOR gain of VOR=dn (n=8, blue circle) and VOR-up (n=8, red circle) group during training and consolidation. In the right panel of (A) and (C), vertical and horizontal scale bars denote 10°/s and 0.5 sec, respectively. Each gain value was normalized by the gain at 0 min in (B) and (D). All data is expressed as the mean ± SEM. A linear mixed model post hoc Tukey test was used to test the statistical significance in pairwise comparison between 0 min and each checkpoint (* p<0.05, ** p<0.01, *** p<0.001). The n.s. means p>0.05 in pairwise comparison of gains among at 50 min, +1 hr, and +24 hrs.

A

Total ID:
6623 protein groups

TMT set.1   416   TMT set.2
386   298
              4801
268   250
              204
          TMT set.3

B

Cytoskeleton (4.42%)
Endoplasmic reticulum (4.18%)
Golgi (3.65%)
Endosome (2.53%)
Extracellular (1.98%)
Chromosome (1.45%)
Organelle lumen (1.36%)
Cell surface (1.34%)
Vacuole (1.25%)
Ribosome (1.12%)
Spiceosomal complex (0.89%)
Proteasome (0.37%)

Cytosol (6.46%)
Mitochondrion (7.30%)
Nucleus (15.33%)
Cytoplasm (19.83%)
Membrane (22.23%)

C

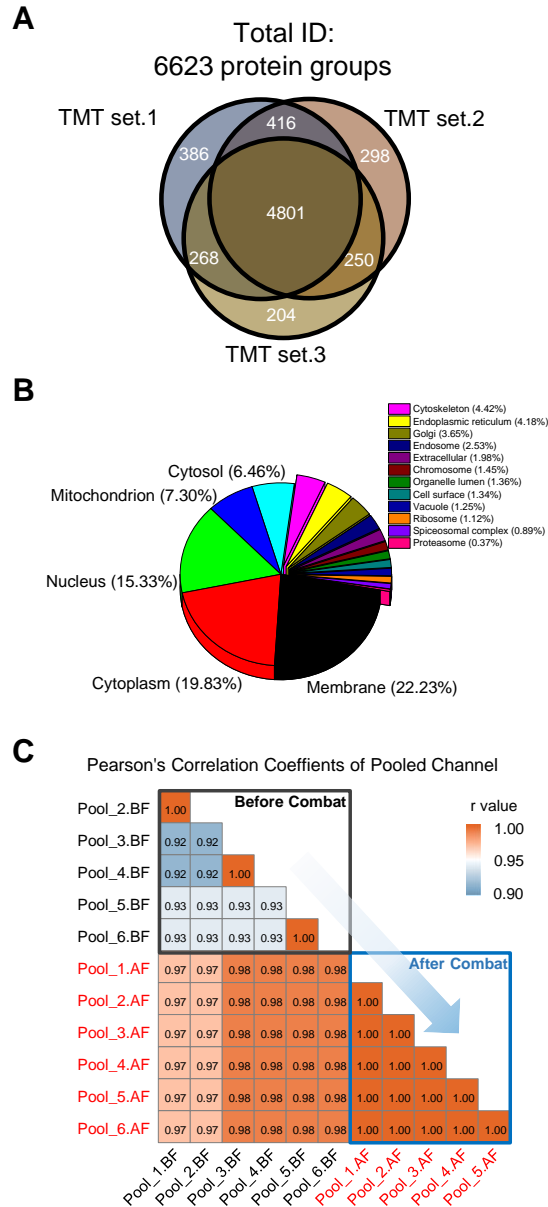Pearson's Correlation Coeffients of Pooled Channel

Figure 1.3. Data assessment of proteomic analysis. (A) Venn diagram showing the number of identified proteins in each experimental set (total 6623 proteins). (B) Gene ontology analysis of identified proteins indicates the proportion of cellular components in flocculus tissues. (C) Before and after batch effect adjustment using Combat algorithm.

29

A

OKR-up
9 proteins

01H

Adnp Fam155a
Psen1 Kank4
Col2a1 Bola1
Aktip

Mcc   Tmpo

Msrb2 Syn2
Engase Itpr1
Bcas1 Sfxn4   Trim9   Nudt18
Sv2c Hspa12b   Mesdc1
Commd2

VOR-dn
11 proteins

VOR-up
4 proteins

B

OKR-up
17 proteins

24H

Cplx2 Pcp2 Psd3
Sncb Tpd52 Snca
Atg3 Fip1l1 Stam
Cttn Agfg1 Stmn1
Pllp Plekha7 Rspry1
Arhgef11 Hist1h2bp

Krt76   Sfr1
Epb41l3   Bgn
                    Ttr
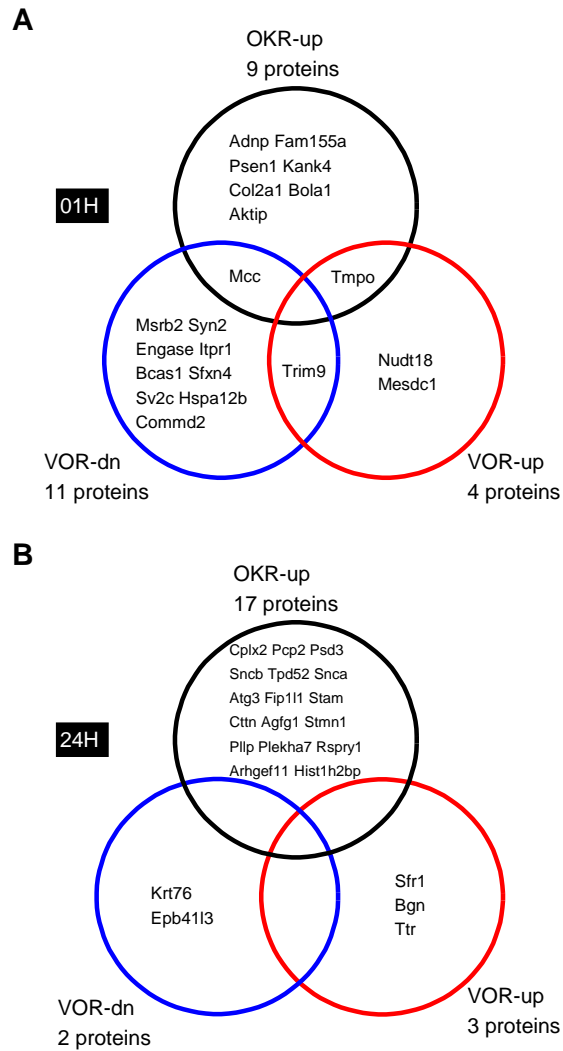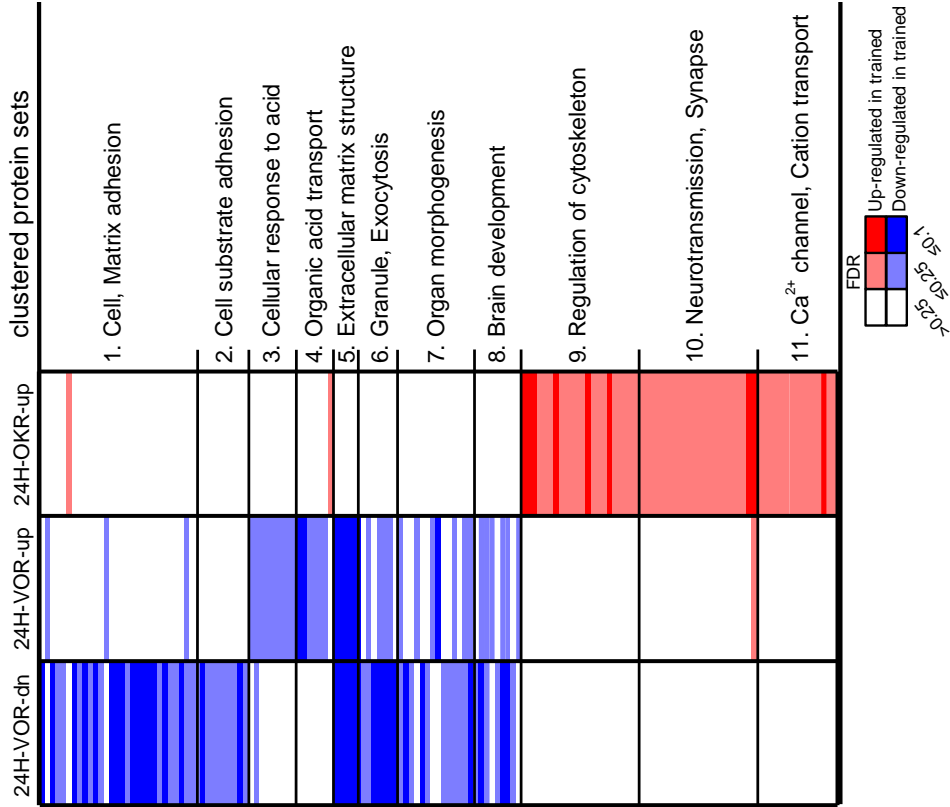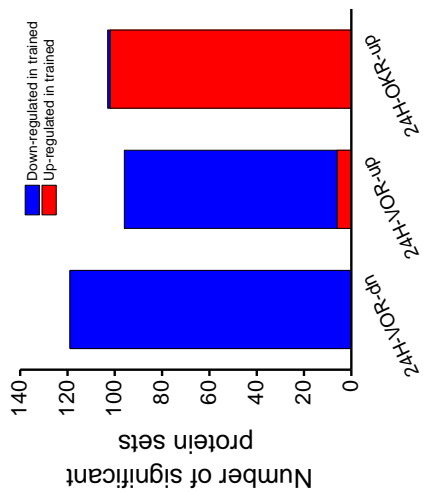
VOR-dn
2 proteins

VOR-up
3 proteins

Figure 1.4. Differential regulation of protein
expression in the cerebellum of three
oculomotor trained mice at 1 hr (A) and 24 hrs
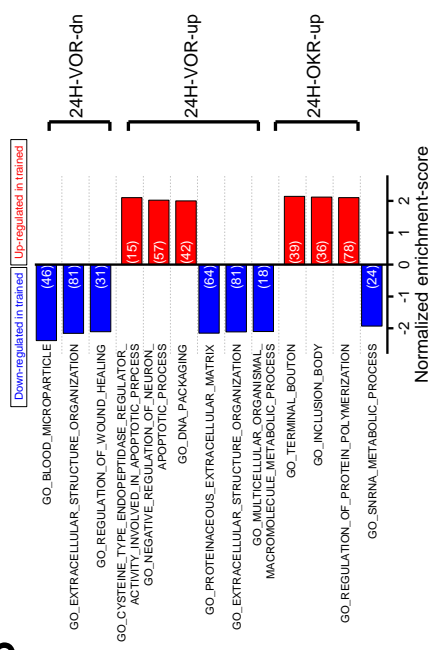(B) after training.

(See legend on next page)

31

(See figure on previous page)

Figure 1.5. Protein set enrichment analysis (PSEA) in LTM group. (A) Number of significantly enriched protein sets (FDR < 0.25) in each pairwise comparison of control and trained groups in LTM group. (B) The top 3 enriched protein sets are represented with normalized enrichment score as a bar graph for each learning paradigm. The numbers in parentheses indicate the number of proteins belonging to a given protein set. (C) Heatmap presenting clustering analysis of PSEA. The scale bars at the bottom right represent FDR of the pairwise comparison. In the PSEA results of each pairwise group, protein sets with high similarity (overlap coefficient > 0.4) were clustered among statistically significant protein sets (11 clusters) (see Materials and Methods). Throughout the figure, deprived and enriched protein sets in trained groups are shown in blue and red, respectively.
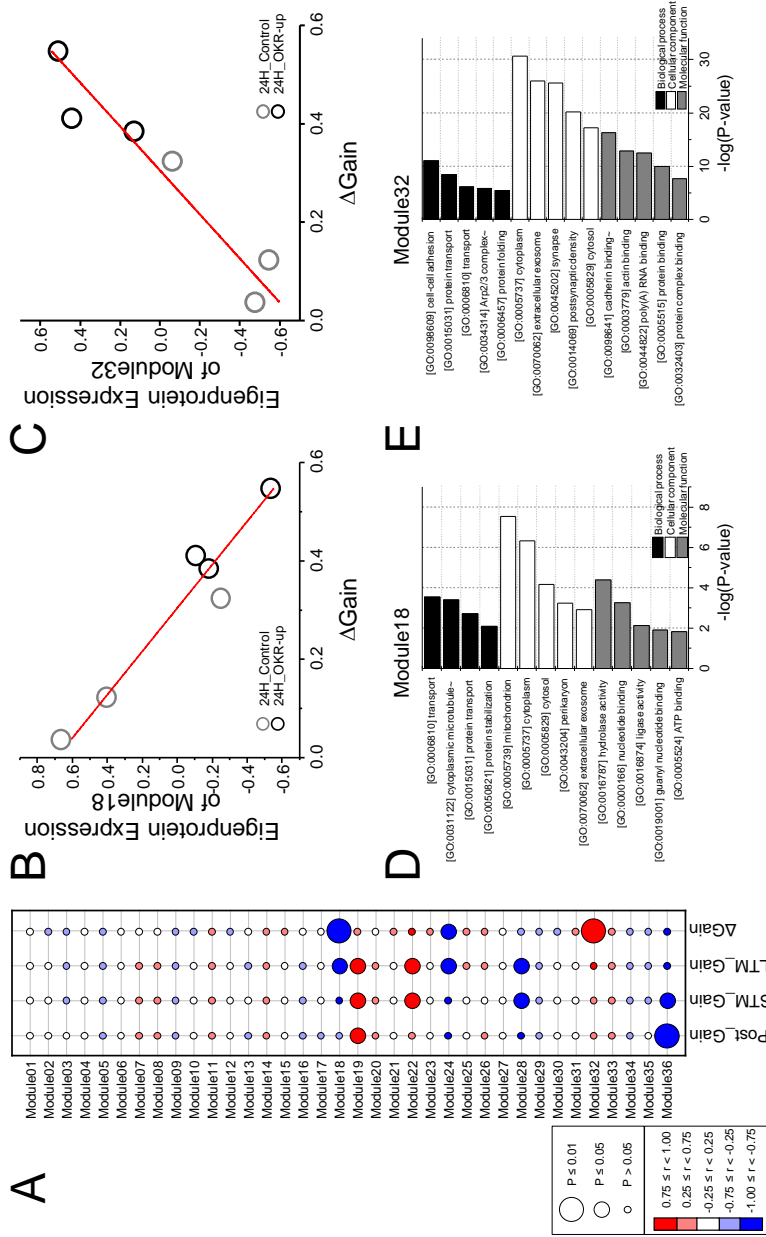
Figure 1.6. Discovery of proteins correlated with oculomotor memory. (A) Module-oculomotor memory association in the OKR-set. Each row corresponds to a module. Each column corresponds to 4 behavioral traits, Post-training gain, STM gain, LTM gain, and ΔGain. In the bubble chart, each cell contains the corresponding correlation coefficients between module and behavioral trait, and their p-values. Correlation between eigenprotein expression and ΔGain in Module18 (B) and Module32 (C). The red lines in (B) and (C) represent the results of linear regression analysis. Top five of GO terms overrepresented in Module18 (D) and Module32 (E) modules. r = Pearson's correlation coefficient, p = P-value.
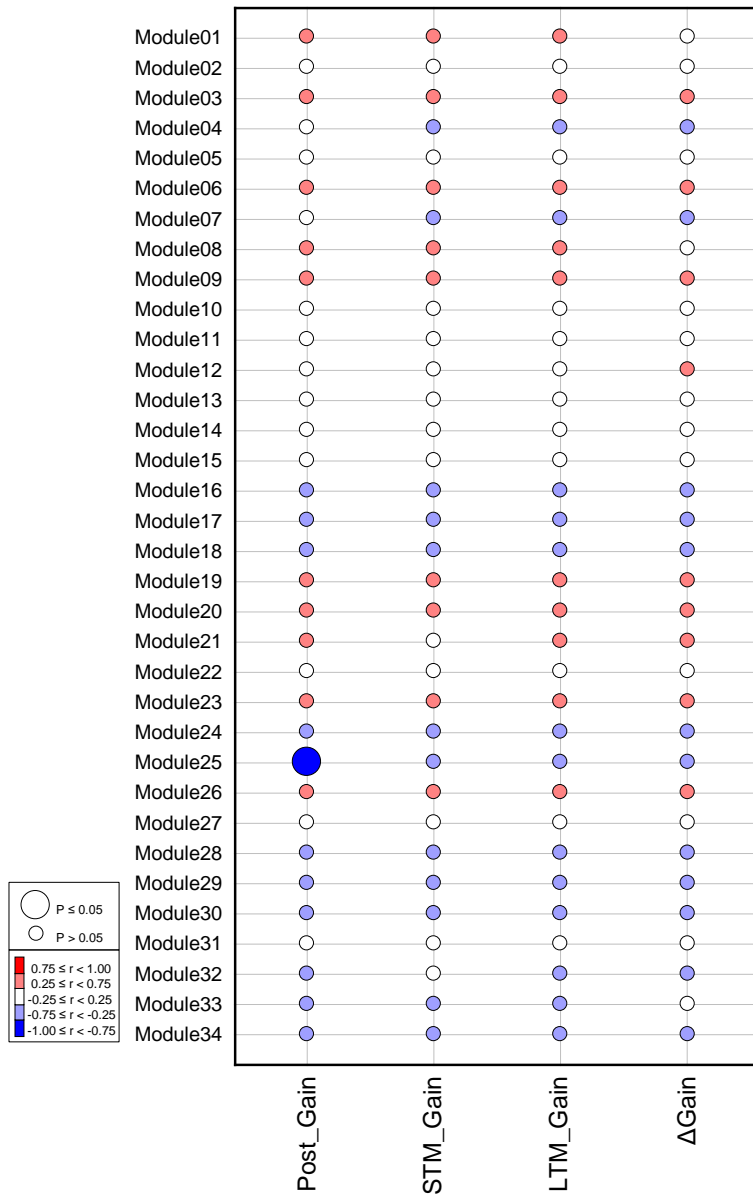
Figure 1.7. Module-VOR memory relationships. Each row corresponds to a module. Each column corresponds to four behavioral traits, Post-training gain, STM gain, LTM gain, and ΔGain. In the bubble chart, each cell contains the corresponding correlation coefficients between module and behavioral trait, and their p-values.
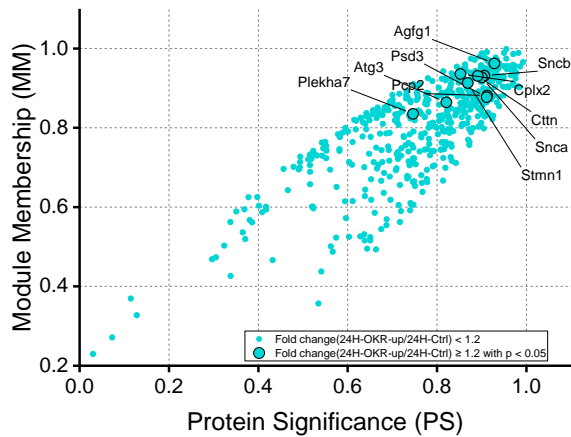
Figure 1.8. Intramodular analysis of Module32 in WGCNA. In Module32, module membership (MM) and protein significance (PS) exhibit a strong positive correlation ($r = 0.71$, $p = 0.01$), implying that the most important proteins in the module (proteins with a high MM) also tend to be highly correlated with ΔGain of OKR learning (high position in PS). Of the 486 proteins in this module, ten proteins had fold changes greater than 1.2 (relative to the control group) with p-value $\leq$ 0.05 (large circles with black boarders).

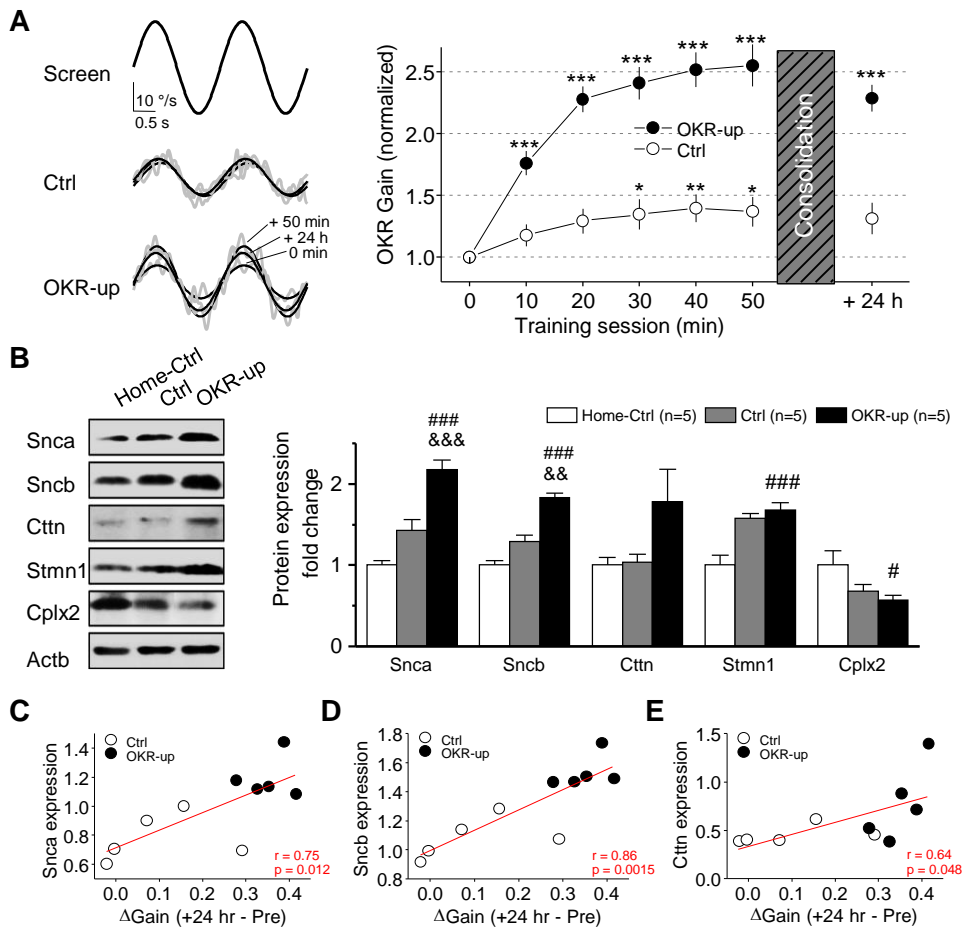Figure 1.9. Biological validation of selected proteins. (A) left) representative eye traces (raw: gray, sine-fitted: black) of Ctrl (middle) and OKR-up (bottom) group in response to oscillation of screen (top) at pre- (0 min) and post-training (+ 50 min), and after 24 hours (+ 24 h). right) Changes in OKR gain of Ctrl and OKR-up group during training and consolidation session. Linear mixed model post hoc Tukey tests used for testing statistical significance between 0 min (pre-training) and each checkpoint. * $p < 0.05$, ** $p < 0.01$ and *** $p < 0.001$. (B) left) Representative Immunoblotting bands of the selected five proteins. right) Averaged results of immunoblotting in Home-Ctrl (white), Ctrl (gray) and OKR-up (black) (n=5 per each group). One-way ANOVA post hoc Bonferroni-test was used for comparisons of mean difference among three groups. # $p < 0.05$, ### $p < 0.001$ between Home-Ctrl and OKR-up groups. && $p < 0.01$, &&& $p < 0.001$ between Ctrl and OKR-up groups. (C-E) Scatter plot of ΔGain (learning amount) versus protein expression of Snca (C), Sncb (D), and Cttn (E). The red lines in (C-E) indicate the results of linear regression analysis. The Ctrl and OKR-up groups are displayed as open and closed circles, respectively. Error bars denote the SEM. r = Pearson's correlation coefficient, p = P-value.

36

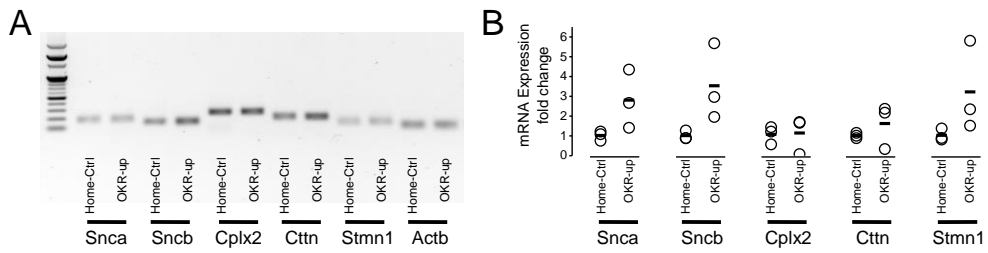Figure 1.10. RT-qPCR Validation of selected proteins. (A) RT-qPCR analysis of *Snca*, *Sncb*, *Cplx2*, *Cttn*, *Stmn1*, and *Actb* mRNA in the cerebellar flocculus from Home-Ctrl and OKR-up groups (n=3 mice per group). (B) Quantification of the ratio of each gene/*Actb* (n=3 per group). Each ratio and the mean value of the ratio within a group are displayed as an open circle and horizontal bar, respectively.
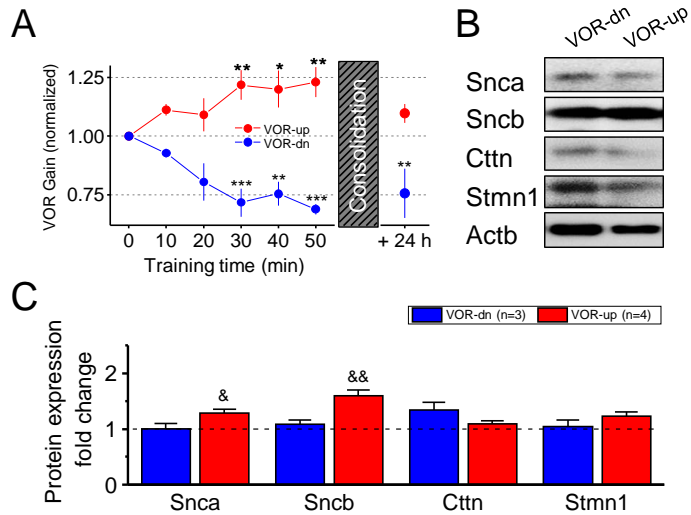
Figure 1.11. Biological validation of selected proteins for the sample from VOR learning groups with memory consolidation of 24 hours. (A) Changes in VOR gain of VOR-dn (n=3) and VOR-up (n=4) groups during training and consolidation sessions. Linear mixed model post hoc Tukey tests used for testing statistical significance between 0 min (pre-training) and each checkpoint. $*$ $p < 0.05$, $**$ $p < 0.01$ and $***$ $p < 0.001$. (B) Representative Immunoblotting bands of 5 proteins (Snca, Sncb, Cttn, Stmn1, and Actb). (C) Averaged results of immunoblotting in VOR-dn (blue, n=3) and VOR-up (red, n=4). Averaged expression of each protein in Home-Ctrl (n=5) display as dashed line. Error bars denote the SEM. One-way ANOVA post hoc Bonferroni-test was used for comparisons of mean difference among VOR-dn, VOR-up, and Home-Ctrl groups. & $p < 0.05$, && $p < 0.01$ between Home-Ctrl and VOR-up group. Data express mean ± SEM.

DISCUSSION

Cerebellar protein networks associated with cerebellum-dependent learning paradigms

In the present study, I hypothesized that direction-selective motor learning would induce distinct expression of proteome-wide network in the cerebellum. In order to test my hypothesis, I conducted proteomics profiling with samples taken from animals that had undergone three different oculomotor learning paradigms. As a result of the bioinformatic analysis, I found that protein sets associated with each learning paradigm were clustered by biological function and the direction of regulation (i.e., up- or down-regulation compared to the control).

In LTM of OKR-up, the expression of proteins responsible for structural or functional changes of neurons was up-regulated compared with that of the Ctrl group, and this up-regulation was not observed in LTM of VOR-up and -dn. It is known that neural plasticity, which is generally accepted as a cellular mechanism underlying learning and memory, is achieved by functional or structural modification of certain synapses, in which regulation of protein expression is essential [4]. My proteomic profiling suggests that OKR-up learning is associated with structural or functional modification of synapses in a variety of neurons in the cerebellar cortex. This result is consistent with previous findings suggesting changes in synaptic receptors or synapse numbers after OKR-up learning [66]. In contrast to the up-regulated pattern of protein sets in LTM of OKR-up, down-regulation of protein sets compared to those in the control group was noted in LTM of VOR-dn and -up groups. Although several clusters of protein sets were co-regulated after VOR learning in both groups, VOR-dn and -up learnings were selectively correlated with 'Cell substrate adhesion' and 'Cellular responses to acid' functions, respectively.

Several lines of evidence support the hypothesis that selective molecular mechanisms are engaged in oppositely directed motor learning [47, 48, 52]. In fact, most of the evidence supporting this bidirectional plasticity mechanism is derived from results showing selective or prominent deficits in VOR-up learning due to genetic or pharmacological manipulation of the cerebellum in mice. Previous research has failed to show selective deficits in VOR-dn learning [57, 60]. As

mentioned above, protein sets related to 'Cell substrate adhesion' function were prominently down-regulated in LTM of VOR-dn. It is well known that this kind of function plays a role in the maintenance of synaptic plasticity and formation of LTM in the brain [78-81]. Hence, it would be interesting to investigate the involvement of 'cell adhesion function' in cerebellum-dependent motor learning, especially in VOR-dn learning. Furthermore, while it is known that VOR and OKR share much of the downstream circuitry for generating and modulating the motor strength of the reflex [36], several studies suggested that the VOR and OKR are performed under different mechanisms [82, 83]. Thus, my findings would facilitate attempts to elucidate the molecular mechanisms that are selectively involved in VOR and OKR learning, respectively.

Discovery of oculomotor learning-related proteins

Learning and the subsequent storage of memory in a brain are known to require alteration in functional or structural synaptic connectivity [4]. Cerebellum-dependent motor learning has also shown to require plasticity at synapses or throughout the neuron in the cerebellum [24, 25, 52]. In accordance with this fact, I note that five of the regulated proteins (Itpr1 [84], Psen1 [85], Cplx2 [86], Stmn1 [87], and Syn2 [88]) have been previously implicated in synaptic plasticity and another three proteins for learning and memory (Trim9 [89], Adnp [90], Snca [91]). Based on the findings from previous studies, I clustered these proteins into two groups, presynaptic and morphological remodeling proteins, in terms of their biological role. For these individual proteins, I review the literature and briefly speculate their role in the formation of oculomotor memory (Supplementary Text at https://pubs.acs.org/doi/10.1021/acs.jproteome.9b00826).

Psen1 [85, 92], Cplx2 [93, 94], Syn2 [88, 95], and Snca [96] are known as presynaptic proteins that interact with synaptic vesicles or other synaptic proteins. In the cerebellum, various presynaptic terminals are known to be actively modulated as a result of synaptic plasticity [24]. Thus, changes in expression of these presynaptic proteins may reflect an involvement of presynaptic plasticity of the cerebellar neural circuit in the formation of oculomotor memory. It has been suggested that other four proteins, Trim9 [89], Stmn1 [97], Adnp [90], and Itpr [98] play a role related to morphological remodeling in neurons. In addition to the functional changes in

40

synapses, structural modification in synapses is also crucial in the consolidation of memory [4]. My result suggest that oculomotor learning may induce structural modification as well as functional changes in synapses in the cerebellum. Of four proteins, Itpr1 is of particular interest because it is known to be involved in synaptic plasticity in PCs as an intracellular Ca^{2+} channel expressed mainly in PCs [99, 100]. The literature suggested a functional role of Itpr1 in OKR-up learning [98], while my results showed that upregulation of Itpr1 occurred following VOR-dn learning. This discrepancy should be resolved in future study.

Despite my suggestion that functional or structural modification at certain synapses would be involved in the formation of three oculomotor memories in the cerebellum, it is hard to speculate specific roles of the identified proteins in each oculomotor paradigm with limited current knowledge. In fact, many of 43 proteins I identified have not been investigated to uncover specific roles for oculomotor learning or synaptic plasticity in the cerebellum. Further studies are needed to explore the physiological roles of these proteins for oculomotor learning and synaptic plasticity in the cerebellum.

Time-dependent changes in cerebellar proteome after oculomotor learning

Cerebellum-dependent oculomotor memory can be divided into STM ($\leqq$ 1 hr) and LTM ($\geqq$ 24 hrs). Previous studies have shown that genetic deletion of specific molecules in the cerebellum had different consequences on STM and LTM [65, 67], suggesting that different molecular mechanisms are engaged in STM and LTM in the cerebellum. Consistently, I found that there is no overlap between 21 and 22 DEPs identified in STM and LTM groups, respectively, suggesting that distinct protein sets are involved in STM and LTM (Figure 1.4, Table 1). In addition, when PSEA was subjected to STM group, changes in protein networks were not evident as those obtained in LTM group. Taken together, I propose that STM formation may trigger acute changes in protein expression around synapses, whereas LTM formation may induce change not only at the individual protein level, but also at global proteome-network levels. It has been reported that learning induces multiple phases of de novo transcription and translation over the course of memory consolidation [101-105]. Thus, my data suggested that DEPs in STM and LTM groups may belong to different

waves of protein expression associated with each phase of memory consolidation, respectively.

The first proteomic profiling of cerebellum-dependent oculomotor memory

This study provides a comprehensive list of molecules that may be involved in cerebellar learning conditions. Over the past 40 years, cellular mechanisms underlying motor learning by the cerebellum have been progressing alongside the development of cellular mechanisms underlying synaptic plasticity in the cerebellar cortex. The single plasticity mechanism initially suggested that motor gain is controlled by cerebellar LTD at the synapse between the parallel fiber (PF) and Purkinje cell (PC) [39, 40, 106]. After the discovery of long-term potentiation (LTP) in the PF-PC synapse [107, 108], an inverse form of LTD, attempts have been made to explain the bidirectional regulation of motor gain by the bidirectional synaptic plasticity at the PF-PC synapse [52, 109, 110]. Based on accumulating evidence, multiple plasticity mechanisms have been proposed, which involves various types of plasticity separately localized or temporally separated beyond the limitations of the bidirectional plasticity (LTD and LTP) mechanism [24, 25]. Given this complexity in cerebellar learning mechanisms and the paucity of studies on relevant proteins, a comprehensive picture of proteome changes during cerebellar learning is necessary.

Recently, proteomic profiling has been used to investigate systemic changes of proteins in the hippocampus and amygdala after memory formation [111, 112], or to investigate the temporal dynamics of memory-related proteins after contextual fear conditioning [105]. Although the quantitative proteomic profiling approach is intensively used in research on the cerebellum [113-117], to my best knowledge, this study is the first attempt to address the molecular nature of cerebellum-dependent memory using quantitative mass spectrometry. My results may catalyze further investigation of the molecular mechanisms governing motor memory formation and consolidation, and targeted proteomics, such as multiple reaction monitoring or parallel reaction monitoring, in cerebellum-dependent motor learning research.

Limitation of the present study

In this study, the difference in protein expression levels between control and trained animals was subtle compared to the results of general quantitative proteomics

studies [118, 119]. Three possibilities may explain the minimal difference in protein expression. The first possible cause is that the compressed difference could further occur by eliminating batch effects to reduce variability while processing data. Proteins found in unadjusted sets show higher mean fold-change than those found in generally adjusted sets. However, the batch adjustment was chosen for these data due to significant batch effects that altered protein ranks that remained even after quantile normalization since increased sensitivity at the expense of specificity was desired for further usage in bioinformatics. Besides, the ratio between conditions in the TMT quantification approach could be suppressed towards the median value due to impure MS1 precursor isolation, leading to lowered accuracy in the quantification of the proteins [120]. To overcome the ratio compression issue, MS3 based quantification approaches have been proposed aiming at the fragmentation of isolated MS2 ions and quantifying the target reporter ions [121]. Nevertheless, the specialized MS instruments are needed for those approaches, not routinely usable yet [122, 123].

Another greater possibility is that the magnitude of the change in protein expression can be underestimated in the complex biological environment of the brain. Although cerebellar flocculus is a crucial region for oculomotor learning [41], it is possible that distinct neuronal subpopulations may be involved in motor memory formation and consolidation. It has been consistently reported that a limited number of neurons was activated during fear conditioning [124]. If similar neuronal selection occurs in the cerebellar cortex during motor memory formation and retention, the expression level of a particular protein may be underestimated in samples containing both participating and non-participating neurons during the memory formation. I speculated that this concern might restrict the spectrum of analysis using DEPs in my result, therefore, I took alternative approaches, such as PSEA and WGCNA, in order to test my hypothesis. As a result of these approaches, I summarized a comprehensive list of proteins that may be involved in different forms of cerebellar learning, and validated four proteins associated with the oculomotor memory using western blot.

Conclusion

My study is the first proteomic approach to uncover the molecular nature of

cerebellum-dependent motor learning. This research provides a comprehensive and unbiased protein list related cerebellum-dependent motor learning, which differs from previous approaches targeting a small number of selected proteins. Newly identified protein sets will facilitate the discovery of mechanisms that selectively mediate each learning circumstance in terms of consolidation or recalibrating motor gain. Furthermore, my work will be utilized as a potentially important resource for a future investigation using advanced proteomic profiling techniques in the field of cerebellum-dependent motor learning.

Chapter II. Suppressed Intrinsic and Synaptic Excitability of Cerebellar Purkinje Cells Following Optokinetic Learning in Mice

INTRODUCTION

The optokinetic response (OKR) is a reflexive eye movement that follows the motion of the visual field, which stabilizes an image on the retina. The OKR is exhibited to adapt to changes in the environment throughout life, which is a type of motor learning. The cerebellum is well-known to participate in this adaptation as an adaptive controller [36]. In optokinetic learning, the cerebellum directly receives the error signal generated in the retina via the accessory optic tract and relays the integrated information to the vestibular nuclei to adapt the oculomotor strength [36].

The cerebellar Purkinje cell (PC) lies in the center of the adaptive controlling unit. PCs are the sole output of the cerebellum that converge two primary afferent pathways, the mossy fiber-parallel fiber (MF-PF) pathway carrying vestibular signals and climbing fiber (CF) carrying the error signal, in their dendrites. Despite the significance of PCs in neural circuitry modulating OKR, attempts to elucidate the physiological role of PCs in optokinetic learning are still lacking. An exceptional study was carried by Inoshita and Hirano (2018) [29]. The authors reported the amplitude of excitatory postsynaptic current at PF-PF was decreased and induction of long-term depression (LTD) was suppressed in wild-type mice underwent optokinetic learning, however, basal electrophysiological properties of PCs has not been tested in this learning paradigm.

Here, I asked whether changes in the intrinsic and synaptic excitability of cerebellar PC are accompanied by optokinetic learning. To address this question, I utilized an ex vivo approach, in which whole-cell patch-clamp recordings were performed from PCs in acute cerebellar slices prepared from mice that underwent OKR learning of 50 min. Comparing the electrophysiological properties of cerebellar PCs between the control and learned groups, I found that PCs from the learned group showed a significant decrease in the firing rate in response to the intracellular depolarizing current injection and a greater rheobase current compared with those in the control group. Moreover, optokinetic learning weakened excitatory synaptic transmission at PF-PC synapses by decreasing presynaptic release probability. Taken together, my result indicates that optokinetic learning dampens neuronal excitability of cerebellar PCs at both intrinsic and synaptic levels, suggesting the engagement of multiple plasticity, which underlies cerebellum-dependent oculomotor learning.

MATERIALS AND METHODS

Animal

C57BL6/J male mice aged 7- to 9-week-old were used. Animals were housed with food and water available ad libitum under a 12 hours light/dark cycle. All animal use was in accordance with protocols approved by the Animal Care and Use Committee of Seoul National University College of Medicine.

Behavioral test

Surgical procedure. The whole surgical process was done under isoflurane anesthesia. In order to restrain the mouse's head during a behavioral test, a headpost was mounted with two M2 nuts, four screws (M1.2 x 5.5), and dental cement (Super bond C&B, Sun Medical, Japan). Nuts were placed approximately on the lambda and bregma of the skull, and screws were implanted beside the nuts. Finally, dental cement was applied between the nuts and screws following manufacturer's instruction. Mice were given for at least 24 hours after surgery.

Apparatus for behavioral tests. Behavioral tests were conducted using the previously described apparatus [70]. Optokinetic stimulation was generated by a cylindrical screen (diameter 50 cm) with vertical black and white stripes. Right eye movement was monitored with a high-speed CCD camera (VGA-210, Imperx, USA) under infrared illumination. The whole system was controlled and monitored by custom-written LabVIEW (National Instrument, USA) code.

Learning protocol. Before the start of the learning session, OKR was measured under sinusoidal oscillation of the screen with a rotation amplitude of 5 deg and a rotation frequency of 0.5 Hz. After baseline recording, a 50 min learning session was run under the same optokinetic stimulation of the baseline recording. Immediately after, OKR was measured again.

Data analysis. Rotational traces of the pupil were calculated from the raw data using the procedure reported by Stahl et al. (2000) [69]. The recorded stimulus (movement of the screen) and response (evoked eye movement) were smoothed and fitted to sine curves. Finally, I obtained the gain of OKR, a ratio of the eye response

to the visual stimulus. For all computational and management procedures of the data, I used VOG Analysis Pack, a custom-built video-oculography (VOG) data analysis tool written by LabVIEW (https://github.com/parkgilbong/VOG_Analysis_Pack)
.

Slice Preparation

Mice were anesthetized with isoflurane, then decapitated. Once the brains were extracted, using a vibratome (VT1200, Leica), coronal cerebellar slices (250μm thick) were obtained. The slices were cut in a chamber filled with ice-cold cutting solution, NMDG-HEPES, composed of the following (in mM): 2.5 KCl, 1.25 NaH_2PO_4, 93 NMDG, 30 $NaHCO_3$, 20 HEPES, 25 glucose, 5 sodium ascorbate, 2 Thiourea, 3 sodium pyruvate, 12 L-acetyl-cysteine, 10 $MgSO_4 \cdot 7H_2O$ and $CaCl_2 \cdot 2H_2O$ bubbled with 95% O_2 and 5% CO_2. Once the brains were completely sliced, those slices were immediately put into an artificial CSF (ACSF) composed of the following (in mM): 125 NaCl, 2.5 KCl, 1 $MgCl_2$, 2 $CaCl_2$, 1.25 NaH_2PO_4, 26 $NaHCO_3$ and 10 glucose bubbled with 95% O2 and 5% CO2. For the recovery, slices were incubated at 32℃ for 15 minutes, and then 1 hour at room temperature.

Electrophysiology

A cerebellar slice was placed in a submerged chamber on the stage of a microscope (BX 50WI, Olympus Optical, Japan) and perfused with ACSF. Data were collected using Multiclamp 700B (Molecular Devices, USA) and Digidata 1440A (Molecular Devices, USA) with the sampling frequency of 10-20 kHz and filtering frequency of 2kHz. For assessment of the intrinsic excitability, the whole-cell current-clamp recordings were performed from PCs in the flocculus at 32℃ using the recording patch pipettes (2.5-3.5 MΩ) filled with internal solution containing the following (in mM): 9 KCl, 10 KOH, 120 K-gluconate, 3.48 $MgCl_2$, 10 HEPES, 4 NaCl, 4 Na_2ATP, 0.4 Na_3GTP, and 17.5 sucrose, pH 7.25. All of the current-clamp recordings were conducted within the ACSF containing 100 μM picrotoxin (Sigma-Aldrich, USA) and 10 μM NBQX (2,3-dihydroxy-6-nitro-7-sulfamoyl-benzo(f)quinoxaline) (Tocris Bioscience, UK) to block inhibitory and excitatory synaptic inputs, respectively. During the current-clamp recording, the membrane potential was maintained at -70 mV. Neurons in which the holding current was exceeded 600 pA were excluded from the analysis. To evaluate the PC excitability, 500 ms-long depolarizing currents were

injected in PCs from +100 to +1200 pA with increments of 100 pA, and the mean firing rate was calculated based on the number of evoked APs in response to a depolarizing current injection. The amplitude of post-burst afterhyperpolarization (PB-AHP) was measured as the difference between the baseline before the current injection and the negative peak potential following the spiking response of PC. The input resistance (R_{in}) was determined by measuring the difference between the baseline and the maximal negative voltage during hyperpolarizing current injection (from -600 pa to -300 pA with increments of 100 pA) of 500 msec duration. The membrane capacitance (C_m) was calculated by dividing the time constant (t) from the exponential curve fitting. All whole-cell current-clamp recording data were analyzed and managed using IntrinsicVIEW Analysis Pack [125].

For the analysis of single action potentials (APs), brief depolarizing currents with a duration of 50 msec were injected in PCs with increments of 10 pA until the first AP fires. The rheobase current was defined as the minimum current magnitude required to generate an AP. The voltage threshold of AP was defined by measuring the membrane potential at which its 1st derivatives exceeded 5 mV/ms. The differences between the AP threshold and the positive, and the negative peak of the trace were defined as the AP amplitude and the AHP amplitude, respectively.

To test the influence of optokinetic learning on excitatory synaptic transmission in PCs, evoked and spontaneous excitatory postsynaptic currents (eEPSC and sEPSC) were recorded in a voltage-clamp configuration within the oxygenated ACSF containing 100 μM picrotoxin (Sigma-Aldrich, USA). A whole-cell recording of PCs was made at 32°C using patch pipettes of 2-3 MΩ filled with internal solution containing the following (in mM): 140 CsCl, 4 NaCl, 0.5 $CaCl_2$, 10 HEPES, 2 MgATP, and 5 EGTA, pH 7.3. The membrane potential of neurons was held at -70 mV. For recording eEPSC, a stimulating electrode was placed in the middle of the molecular layer. PF stimulation intensity ranged from 10 to 50 μA with 10 μA increments. Within a stimulation intensity, five sweeps were recorded and averaged. To examine the paired pulse ratio (PPR) of EPSC amplitude, paired eEPSCs were induced by paired-pulse stimulation at intervals of 50, 100, 150, and 200 ms. The mean of PPR was calculated from five sweeps in a cell. The sEPSC events were detected with Minhee Analysis Package (RRID:SCR_021250) [126] using a

detection threshold of 10 pA.

Statistics

All statistical computing was performed using R Project for Statistical Computing (RRID:SCR_001905), OriginPro (RRID:SCR_014212), IntrinsicVIEW Analysis Pack, or Minhee Analysis Package (RRID:SCR_021250). For the assessment of learning effect in OKR learning, a paired t-test was used. To compare electrophysiological properties between the control and learned groups, an independent t-test and linear mixed model post-hoc Tukey test were used for the analysis of single and repeated measurement data, respectively. Kolmogorov-Smirnov (K-S) tests were used for comparisons between cumulative probabilities of sEPSC data. For comparison among three independent groups, one-way ANOVA with post-hoc Tukey test was used. All data are presented as mean ± SEM.

RESULTS

Oculomotor Learning in Mice

I performed OKR training in C57BL/6 mice (n=9). Mice were subjected to continuous oscillation (0.5 Hz, ± 5 °, peak-to-peak) of optokinetic screen for 50 minutes in a head-fixed condition (Figure 2.1A, top). OKR gain was measured at two particular temporal intervals: 0 and 50 mins, from the beginning until the end (Figure 1A, bottom). As expected, OKR gain was significantly increased after the completion of the training session (Figure 2.1B, paired t-test, t = -6.87, df = 8, p < 0.001).

Firing Patterns of Floccular Purkinje cells in the Cerebellum

After the completion of the OKR learning, I prepared acute coronal cerebellar slices and the whole-cell patch-clamp recordings were performed from PCs in the cerebellums of the control and learned groups. I recorded from a total of 156 floccular PCs across 6 mice. It is known that distinct firing responses existed in cerebellar PCs in response to the somatic current injection in rats [127]. In my recording, the somatic current injection to PCs revealed two different firing patterns: initial spiking (32 neurons) and regular spiking (124 neurons) (Figure 2.2A). An initial spiking is characterized by an occurrence of single or a few spikes as a response to the depolarizing current injection while a regular spiking pattern is described with a continuous train of action potentials. In the control group, 71 neurons (79.8%) showed the regular spiking pattern, while the other 18 neurons exhibited the initial spiking pattern (20.2%). In the learned group, 53 neurons (79.1%) had the regular spiking pattern and the rest (14 neurons, 20.9%) fired initial spikes (Figure 2.2B). Although the initial spiking pattern has been observed in more than 20% of both groups, further analysis of spiking properties was limited due to the lack of spikes [127]. Therefore, initial spiking neurons were excluded from the analysis.

Reduced Intrinsic Membrane Excitability of Floccular PCs after OKR Learning

To determine whether floccular PCs undergo learning-induced alteration in intrinsic membrane excitability, I injected step currents into PCs in a current-clamp mode (Figure 2.3A). The neurons from the learned group showed significant

reduction in mean firing rate compared with that of neurons in the control group (Figure 2.3B, χ^2 = 29.97, df = 11, p < 0.01, Linear mixed model post hoc Tukey's test). In contrast to the mean firing rate, the amplitude of PB-AHP was not significantly different between two groups (Figure 2.3C). The latency to the 1st AP firing tended to increase in the learned group compared to the control group at +400 pA and more current injection (Figure 2.3D).

An effect of oculomotor learning on passive membrane properties of PCs was assessed by comparing two measurements, the input resistance (R_{in}) and membrane capacitance (C_m) between the control and learned groups. In a current-clamp mode, the peak amplitude of negative voltage deflection was used to measure R_{in} in response to hyperpolarizing current injection. C_m was calculated from the neuronal response to hyperpolarizing voltage step of -5 mV in a voltage-clamp mode. No differences were found when comparing the input resistance and the membrane capacitance between two groups (Figure 2.4A and B; R_{in}, t = 0.80, df = 120, p = 0.42; C_m, t = -0.58, df = 91, p = 0.56, Two sample t-test). The holding current for maintaining membrane potential to -70 mV also did not alter after oculomotor learning (Figure 2.4C; t = -0.04, df = 91, p = 0.96, Two sample t-test).

Comparison of a single AP in PCs from control and learned groups

To look for changes in properties of the AP that could explain the reduction in excitability of PCs, I performed the analysis of a single AP in PCs of both groups. For the analysis of single AP, I injected rectangular current step (duration of 50 ms with 10 pA increments) into PCs to evoke a single AP and measured four AP parameters, the rheobase current, AP threshold, AP amplitude and afterhyperpolarization (AHP) amplitude (Figure 2.5A, See Materials and Methods). The rheobase current after oculomotor learning was significantly increased (Figure 2.5B; t = -2.374, df = 91.3, p < 0.05, Two-sample t-test). Unlike the rheobase current, other three properties, AP threshold, AP amplitude and AHP amplitude, were not altered by oculomotor learning (Figure 2.5C-E; AP threshold, t = -1.13, df = 119, p = 0.26; AP amplitude, t = 0.6, df = 118.98, p = 0.55; AHP amplitude, t = -0.42, df = 119, p = 0.68, Two sample t-test).

No Change in Intrinsic Excitability of Parafloccular PCs after OKR

Learning

Next, I tested whether OKR learning had a broad effect on PCs in the vestibulocerebellum, which is a functionally classified region involving equilibrium and oculomotor functions. I assessed the influence of OKR learning on intrinsic excitability of PCs in paraflocculus (PFL), which is a part of the vestibulocerebellum and is anatomically adjacent to FL (Figure 2.6A).

No differences in mean firing rate and PB-AHP were revealed between control and learned groups (Figure 2.6B and C; mean firing rate, $\chi^2 = 8.61$, df = 11, p = 0.66; PB-AHP, $\chi^2 = 4.32$, df = 11, p = 0.96, Linear mixed model). Furthermore, in the single AP analysis, None of AP parameters were altered by OKR learning (Figure 2.6D-G; AP threshold, t = -0.535, df = 65, p = 0.59; AP amplitude, t = 0.249, df = 65, p = 0.8; AHP amplitude, t = -0.973, df = 50.9, p = 0.34; Rheobase current, t = 0.148, df = 65, p = 0.88, Two sample t-test). Lastly, I found that the input resistance of parafloccular PCs of the learned group did not significantly differ with that of the control group (Figure 2.6H; t = 0.118, df = 65, p = 0.91, Two sample t-test).

Decreased excitatory synaptic transmission in floccular PCs after OKR learning

Many lines of evidence suggested that synaptic plasticity at PF-PC synapse was considered as a primary cellular mechanism for optokinetic learning (Ito, 1989; Hirano, 2013). Based on this hypothesis, it was expected that acute optokinetic learning would lead to a plastic change in excitatory synaptic transmission at PF-PC synapse. Although a previous study already reported a decrease in excitatory synaptic transmission at PF-PC synapses following optokinetic learning [29], eEPSC and sEPSC have not been tested in the wild-type model of optokinetic learning. Therefore, I recorded and analyzed evoked and spontaneous EPSCs at PF-PC synapse to characterize excitatory synaptic properties of PCs.

For eEPSC and sEPSC, I added a sham group as a control group. Animals in the sham group experienced the same as the learned group, such as surgery and restraint, except for a visual stimulation for the learning (Figure 2.7A). To measure eEPSC at PF-PC, a stimulating electrode was placed in the middle of the molecular layer (Figure 2.7B). I found that the learned group showed a reduced eEPSC amplitude compared to the two control groups (control vs. learned, t = 7.596, df = 20, p < 0.001;

sham vs. learned, t = 4.417, df = 20, p < 0.05, Two-way Repeated-Measures ANOVA post-hoc Tukey test), while the control and sham groups exhibited no difference in the amplitude of eEPSC as a stimulating intensity increased (control vs. sham, t = 3.178, df = 20, p > 0.05, Two-way Repeated-Measures ANOVA post-hoc Tukey test) (Figure 2.7C and D).

I also examined whether the optokinetic learning alters spontaneous excitatory synaptic transmission (Figure 2.8A). Interestingly, acute optokinetic learning shifted the distribution of the interevent intervals (IEIs) to the right (control vs. learned, Z = 6.792, p < 0.001; sham vs. learned, Z = 6.859, p < 0.001, K-S test) and significantly reduced the mean frequency of sEPSCs (control vs. learned, q = 4.114, p < 0.05; sham vs. learned, q = 4.585, p < 0.01, One-way ANOVA post-hoc Tukey test) (Figure 2.8B). The distribution of total sEPSC amplitude significantly shifted to the left after the learning (control vs. learned, Z = 2.541, p < 0.001; sham vs. learned, Z = 2.468, p < 0.001, K-S test), however, this tend did not reach statistical significance in the comparison of the mean sEPSC amplitude between groups (control vs. learned, q = 2.099, p > 0.05; sham vs. learned, q = 1.652, p > 0.05, One-way ANOVA post-hoc Tukey test) (Figure 2.8C).

Increased paired pulse ratio of eEPSC in floccular PCs after OKR learning

Finally, I examined whether the release probability at PF-PC synapses was affected by optokinetic learning. It is well-known that the paired pulse ratio (PPR) of eEPSC amplitude reflects the release probability at a synapse [128, 129]. To measure paired eEPSC, I utilized a paired pulse stimulation with interstimulus intervals of 50, 100, 150, and 200 ms (Figure 2.9A). As a result, I found that PPR at an interval of 50 ms was significantly elevated in the learned group compared with the two control groups (control vs. learned, t = 8.096, df = 186, p < 0.001; sham vs. learned, t = 80804, df = 186, p < 0.001, Two-way Repeated-Measures ANOVA post-hoc Tukey test) (Figure 2.9B). With respect to the rest of interstimulus intervals, PPR was higher in the learned group than in the control group, but this difference was not statistical significance.

Taken together, my result suggested that acute optokinetic learning induced a decrease in excitatory synaptic gain at PF-PC synapse and that the reduced presynaptic release probability could be attributed to the cause.
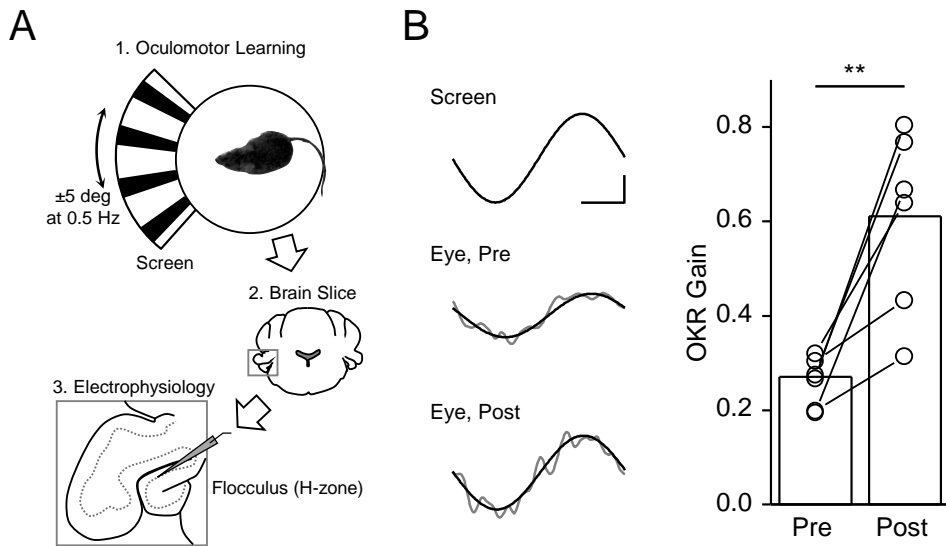
Figure 2.1. Optokinetic learning and ex vivo recording paradigms. (A) Experimental design. Mice were subjected to oculomotor training for 50 min by rotating an optokinetic screen displaying vertically aligned white and black stripes (top). After learning, cerebellar slices were prepared (middle) and whole-cell patch-clamp was performed from the floccular PCs located at the H zone (bottom), The dashed line represents the PC layer. (B) (Left) representative traces of the screen (top), eye movements before (middle) and after (bottom) the learning. In the middle and bottom traces, gray and black lines represent raw and curve-fitted traces, respectively. (Right) Learning-induced increase in OKR gain. Bar graphs indicate the mean value of each time-point. A paired t-test was used for testing statistical significance between two time-points. ** indicates $p<0.01$.
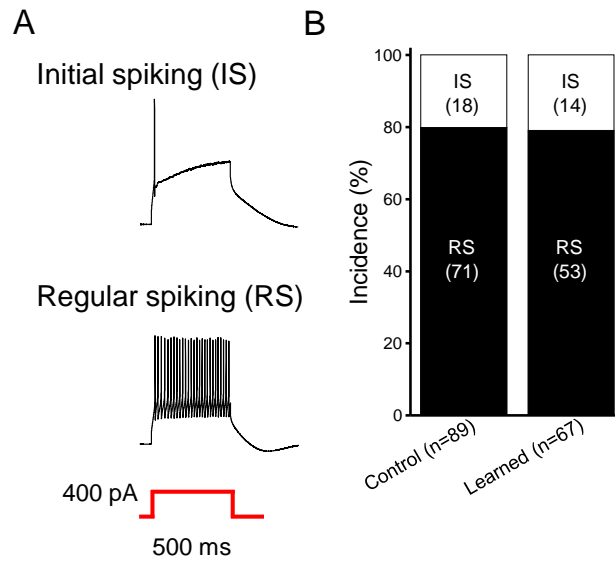
Figure 2.2. Firing patterns of PCs in the cerebellar flocculus. (A) Injection of depolarizing current (bottom) into PCs revealed two kinds of firing pattern, initial spiking (IS, top) and regular spiking (RS, middle). (B) Occurrence of firing patterns was observed similarly between the control and learned groups.
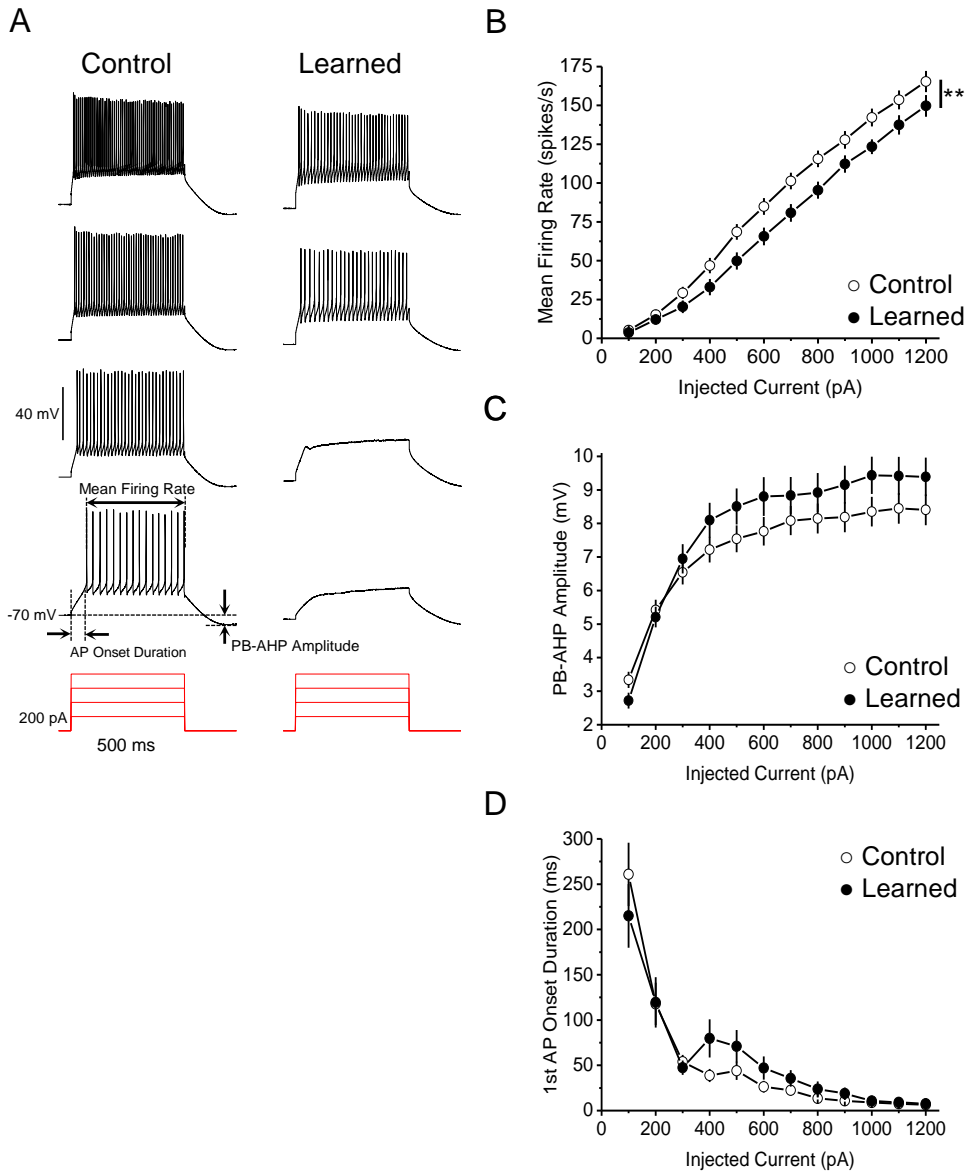
Figure 2.3. Acute oculomotor training suppresses the intrinsic excitability in floccular PCs. (A) Depolarizing current (100 ~ 1200 pA) was injected into floccular PCs of control (left) and learned (right) groups. (B) Mean firing rate, (C) Post burst-afterhyperpolarization (PB-AHP) amplitude, and (D) Latency to the 1st AP firing of the control and learned groups in response to depolarizing current injection. Data represent as mean ± SEM. A linear mixed model post-hoc Tukey test was used for the analysis of repeated measurement data. ** indicates $p < 0.01$.

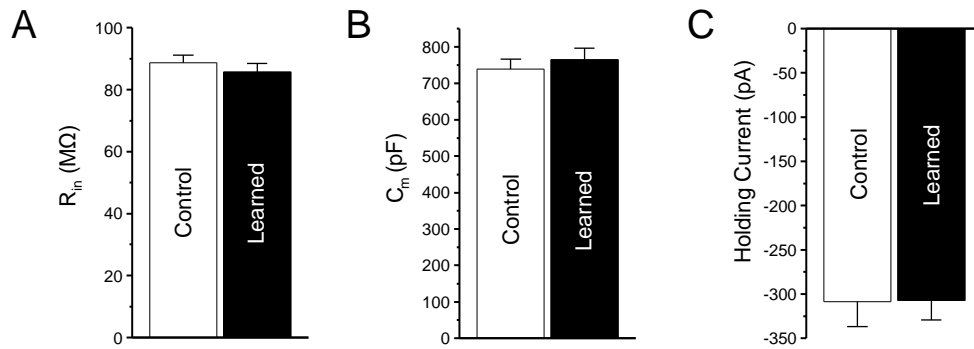Figure 2.4. Comparisons of the passive membrane properties between the control and learned groups. (A) Input resistance (R_{in}) and (B) Membrane capacitance (C_m), and (C) Holding current for maintaining membrane potential to -70 mV are comparable between the control and learned groups. Data represents as mean ± SEM. An independent t-test was used for comparisons of mean difference between the control and learned groups.

Figure 2.5. Single AP analysis in the control and learned groups. (A) Measurement and analysis of individual AP in the control (left) and learned (right) groups. (B) OKR learning increases the rheobase current. (C) AP threshold, (D) AP amplitude, and (E) AHP amplitude are comparable between the groups. Data represents as mean ± SEM. An independent t-test was used for comparison of mean difference between the control and learned groups. * indicates $p < 0.05$.
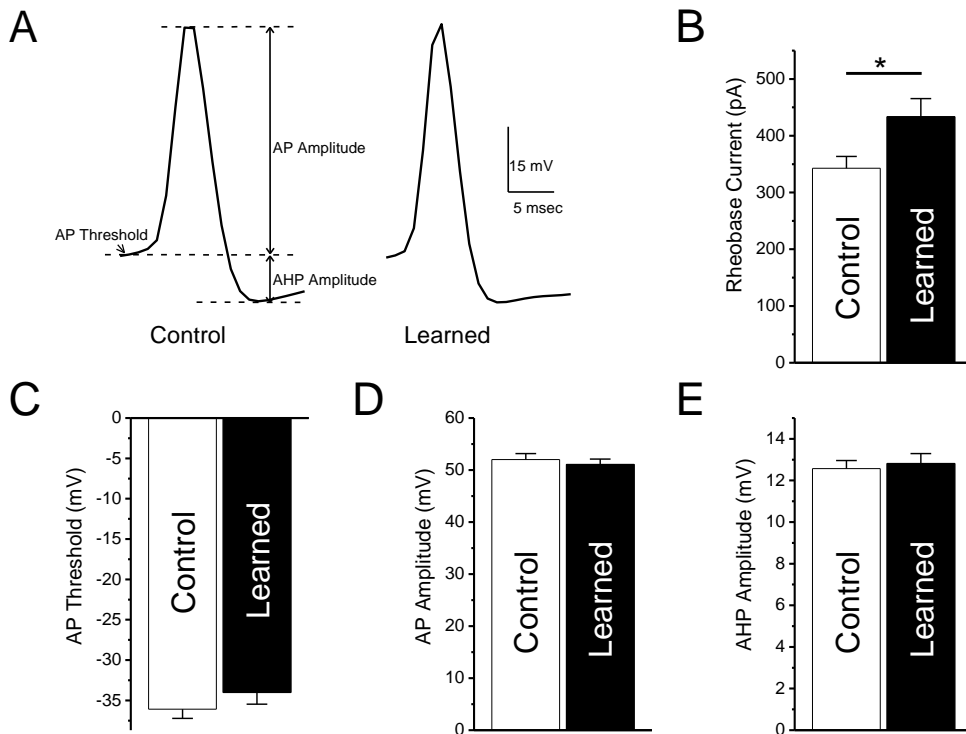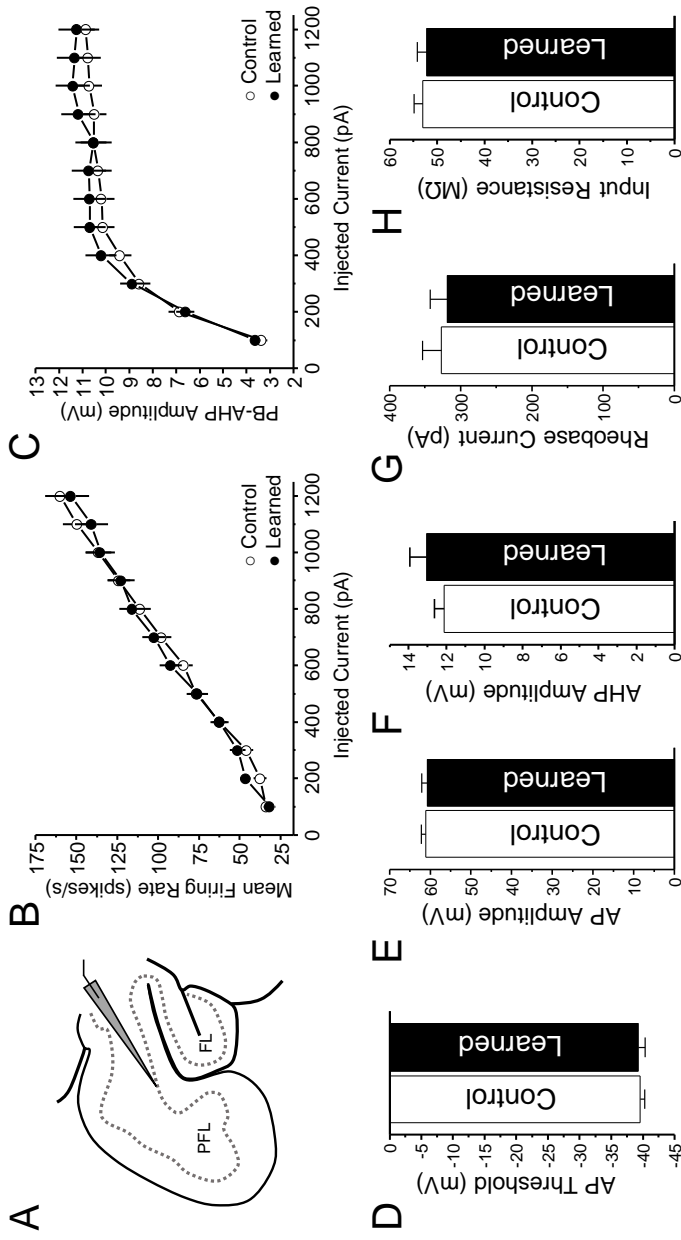
Figure 2.6. Oculomotor training has no effect on the intrinsic excitability of PCs in the paraflocculus (PFL). (A) Schematic illustration of FL and PFL lobes. Dotted line represents the Purkinje cell layer. (B) Mean firing rate and (C) PB-AHP amplitude are comparable between the control and learned groups. No difference in (D) AP threshold, (E) AP amplitude, (F) AHP amplitude, (G) Rheobase current, and (H) Input resistance is found between two groups. In (B) and (C), statistical significance is assessed using a mixed linear model for (B) and (C). In (D)~(H), an independent t-test is used to assess statistical significance. Data represent as mean ± SEM.
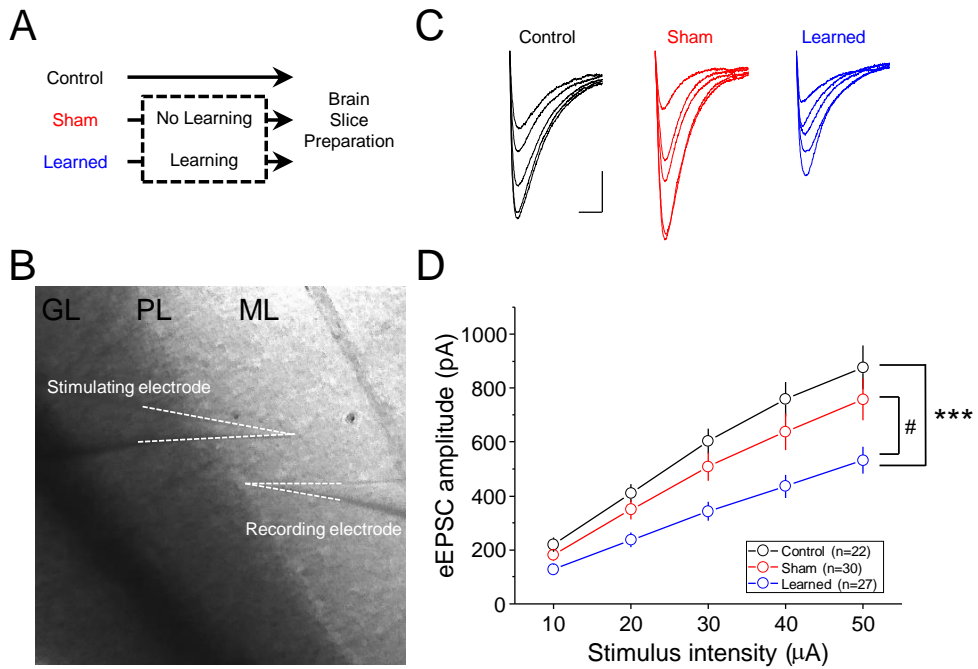
Figure 2.7. Decreased evoked excitatory postsynaptic current (eEPSC) in floccular PCs following optokinetic learning. (A) Animal groups and (B) whole-cell patch-clamp configuration for the assessment of excitatory synaptic transmission at PF-PC synapse after optokinetic learning. GL, granule cell layer; ML, molecular layer; PL, Purkinje cell layer. (C) Representative traces of eEPSCs of the three experimental groups. Statistical significance of differences in eEPSC amplitude among three groups was tested using two-way repeated-measures ANOVA with post-hoc Tukey test. *** indicates $p < 0.001$ in comparison between the control and learned groups. # indicates $p < 0.05$ in comparison between the sham and learned groups.

Figure 2.8. Decreased spontaneous excitatory postsynaptic current (sEPSC) in floccular PCs following optokinetic learning. (A) Representative sEPSC traces in the control (top), sham (middle), and learned (bottom) groups. (B) Cumulative probability plots of interevent intervals of sEPSC in the groups. Inset graph represents the mean sEPSC frequency in the groups. (C) Cumulative probability plots of the sEPSC amplitude. Inset graph depicts the mean sEPSC amplitude in the groups. Throughout the figure, the control, sham, and learned groups illustrate in black, red, and blue colors, respectively. In the inset group, an opened circle and horizontal bar indicate an individual and mean value of each group, respectively. In (B) and (C), Kolmogorov-Smirnov tests were used for comparisons between any pair of cumulative probabilities of sEPSC data. In the inset graphs, one-way ANOVA with post-hoc Tukey test was used to test statistical significance of mean difference among the control, sham, and learned groups. * indicates $p < 0.05$ in comparison between the control and learned groups. ## indicates $p < 0.01$ in comparison between the control and learned groups. N.S indicates $p > 0.05$ in comparison between groups.
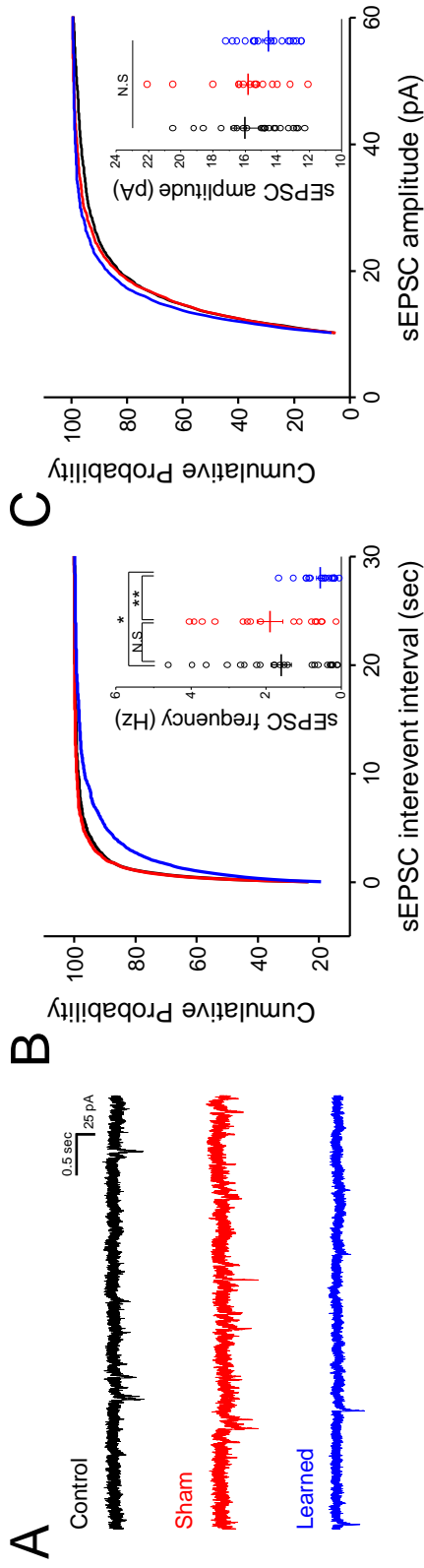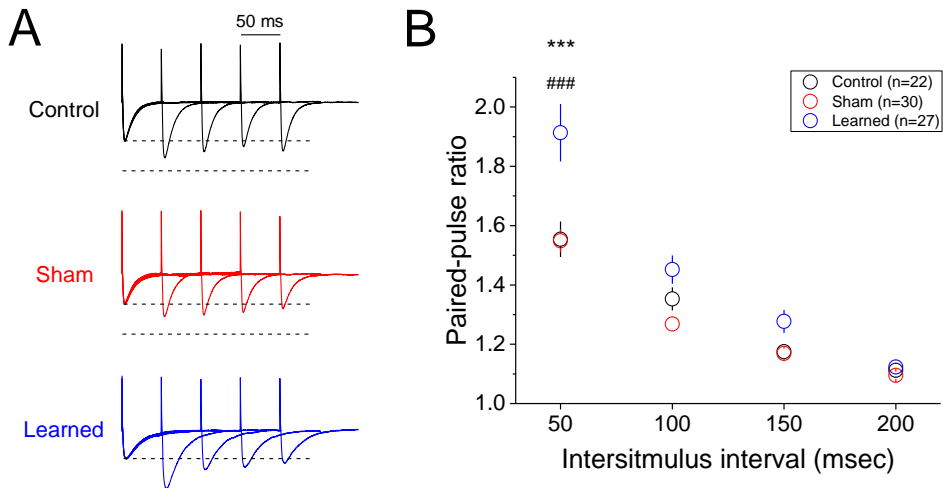
Figure 2.9. Comparison of paired pulse ratio (PPR) in the control, sham, and learned groups. (A) Representative PPR traces in the control (top), sham (middle), and learned (bottom) groups. The eEPSCs in each group were scaled by the first eEPSC amplitude. Dashed lines in each row indicate 1 (top) and 2 times (bottom) the amplitude of the first eEPSC. (B) PPR of eEPSCs with 50, 100, 150, and 200 intervals. The control, sham, and learned groups illustrate in black, red, and blue colors, respectively. Data represent as mean ± SEM. Statistical significance of differences in PPR among three groups was tested using two-way repeated-measures ANOVA with post-hoc Tukey test. *** indicates $p < 0.001$ in comparison between the control and learned groups. ### indicates $p < 0.001$ in comparison between the sham and learned groups.
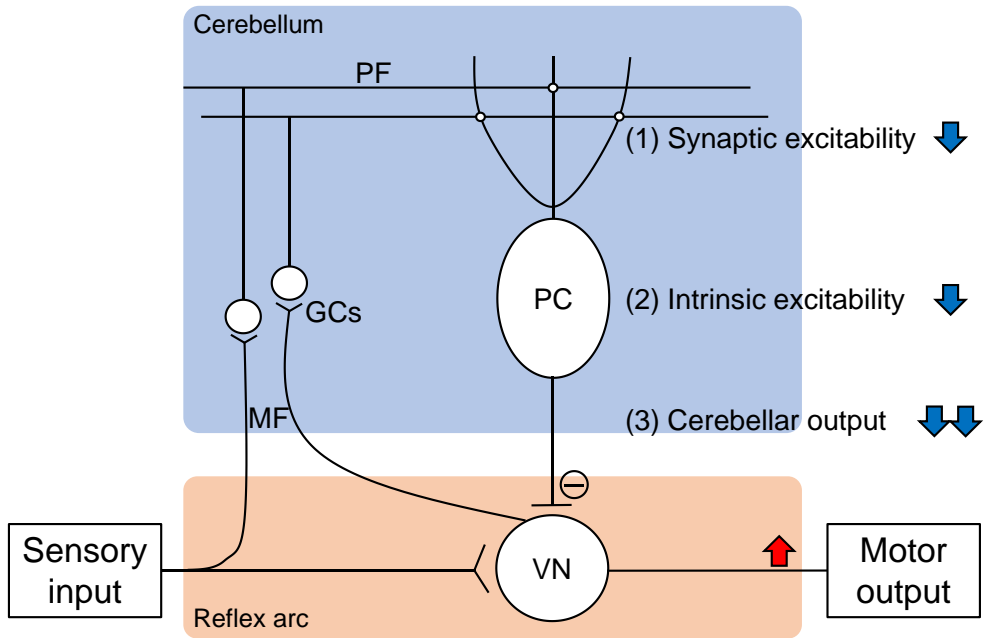
Figure 2.10. Functional implication for the decreased synaptic and intrinsic excitability of the cerebellar Purkinje cells following optokinetic learning. The finding in the present study suggests that presynaptic depression at PF-PC synapse (1) and a decrease in PC intrinsic excitability (2) may occur in the cerebellar cortex after cerebellum-dependent motor learning and may cooperate to facilitate a decrease in cerebellar output to the vestibular nucleus (3). As a result, the OKR gain would be enhanced (red arrow). GC, Granule cell; MF, Mossy fiber; PC, Purkinje cell; PF, Parallel fiber; VN, Vestibular nucleus.

DISCUSSION

Intrinsic excitability is reduced in cerebellar Purkinje cells after oculomotor learning

In the present study, I showed a significant decrease in the firing rate of the cerebellar PC in response to the intracellular injection of depolarizing current after 50 minutes of optokinetic learning. Further single AP analysis found that the rheobase current was increased in the learning group, while AP threshold, AP amplitude, and AHP amplitude did not differ significantly between the control and learned groups. Taken my results together, it would be expected that a decrease in the intrinsic excitability was induced in the floccular PC of the learned group by an increase in the current threshold for generating AP.

It is known that there are various ion channels, such as A-type, D-type, and M-type K^+ channels, activated at the subthreshold potential, and their activities have an effect on the firing properties of neurons [38]. Of these ion channels, the A-type K^+ channels are known to be highly expressed in the cerebellar PC [130]. Previous studies have shown that as the I_A conductance increased in an activity-dependent manner, the acceleration of AP spikes was decreased, therefore, the overall intrinsic excitability of neurons was reduced [131]. Another study suggests that cerebellar PCs exhibited increased dendritic excitability after eye-blink conditioning due to the downregulation of I_A conductance [28].

Furthermore, in response to the depolarizing current injection, the latency to the 1st AP tended to increase compared to that of the control group at + 400 pA and greater steps after optokinetic learning. A delayed firing phenotype of the cerebellar PC has been reported by Kim and colleagues in 2012 [127]. In this study, it has been suggested that the delayed firing phenotype of the PC was associated with 4-AP-sensitive ion conductance and the neurons exhibiting the delayed firing were lower intrinsic excitability than regular spiking neurons. Although I did not subdivide into another firing pattern after the classification between the regular and initial firings in my experiment, my result suggests the possibility of increased I_A conductance in the cerebellar PC after optokinetic learning, resulting in an increase in the number of neurons showing a delayed firing phenotype.

Another possibility is a change in ion conductance of the D-type K^+ channel. The D-type K^+ channels, known to be expressed in cerebellar PCs, play an electrophysiological role similar to the A-type K^+ channels [132]. Recent reports have shown that the activity-dependent regulation of I_D conductance occurs in hippocampal pyramidal neurons [133]. In this study, the authors reported a decrease in the number of APs in response to depolarizing current injection after the theta-burst stimulation and an increase in the latency to the first AP, which is consistent with my findings. However, the authors also reported that the input resistance of neurons decreased after the stimulation, which did not change in my study.

The intrinsic excitability of neurons is influenced by the conductance of voltage-dependent ion channels that affects the passive and active membrane properties of the neuron. Although in the present study, I observed overall changes in the intrinsic excitability of cerebellar PCs after motor learning, a further attempt should be made to determine the ion conductance that mediates the reduced excitability of cerebellar PCs after optokinetic learning. If optokinetic learning caused a plastic change in the intrinsic excitability of cerebellar PCs, the question of which intracellular signaling cascade mediates the changes should be addressed.

Involvement of the floccular lobe in the formation of oculomotor memory

In the present study, I compared the intrinsic excitability of parafloccular PCs between the control and learned groups besides the assessment of the intrinsic excitability of floccular PCs. PFL is located next to FL and, along with FL, is a subregion of the vestibulocerebellum. Several studies have tested the involvement of parafloccular PCs along with PCs in FL after optokinetic learning [29, 66, 134]. As a result, it has been suggested that parafloccular PCs may not be directly linked with optokinetic learning in terms of simple spike modulation [134], structural modification [66] and synaptic plasticity at pf-PC synapse [29]. In accordance with the previous results, my result suggests that the intrinsic excitability of parafloccular PCs also may not be linked with optokinetic learning.

Discovery of presynaptic plasticity at PF-PC synapses in cerebellum-dependent motor learning

Since the cerebellar LTD hypothesis suggested as a primary cellular mechanism

for cerebellum-dependent motor learning [41], a number of studies have attempted to elucidate the relationship between the synaptic plasticity and cerebellar learning. As a result of the intensive attempts, long-term depression (LTD) and potentiation (LTP) were discovered in both pre- and postsynapse at PF-PC synapses [107-109, 135-138].

In addition to the discoveries of in vitro synaptic mechanisms, other efforts have been made to validate the physiological or behavioral relevance of the proposed plasticity mechanism. Of the proposed mechanisms, postsynaptic LTP and LTD at PF-PC synapse have been extensively demonstrated by the studies using the animal model in which the synaptic plasticity was suppressed genetically or pharmacologically [42, 43, 45, 47, 57, 58, 60, 62]. In contrast to the abundant supporting evidence related to postsynaptic plasticity mechanisms, there is a lack of evidence to support the behavioral relevance of presynaptic plasticity at PF-PC synapse.

In the present study, I found decreased eEPSC and sEPSC in the cerebellar flocculus prepared from the mice that underwent 50 min of optokinetic learning. I further revealed that an increase in PPR occurred at PF-PC synapse in the learned group, compared to the control group. Given that PPR reflects the release probability at a synapse [128, 129], my result suggests that acute optokinetic learning suppresses synaptic transmission at PF-PC synapse by reducing the presynaptic release probability. An ex vivo approach using animals undergoing a physiological learning paradigm has been used to elucidate possible cellular mechanisms in the formation and retention of memory in the brain [139]. It is to note that my finding is a pioneering result which suggests presynaptic plasticity at PF-PC synapse may be engaged in a physiological learning circumstance. Thus, my work would be a potential clue for discovering the presynaptic plasticity mechanism governing cerebellum-dependent motor learning in the future.

Implication of this study

The OKR system consists of the optokinetic sensory system, relay system between sensory and motor systems, and oculomotor system, which is well-known as a typical feedback control system [36]. The cerebellum actively engages in this reflex arc to improve the performance of OKR. According to the cerebellar LTD hypothesis,

the increase in OKR gain can be explained by the decrease in synaptic strength of the cerebellar PCs, which has direct influence on the reflex arc. While the cerebellar LTD hypothesis has been mainly supported by the studies focused on LTD at postsynapse of PF-PC synapse, my finding suggests that a presynaptic depression may occur at PF-PC synapse after cerebellum-dependent motor learning. Consequently, this LTD-like plasticity may contribute to strengthening OKR gain in cooperation with the postsynaptic LTD at PF-PC synapse (Figure 2.10).

To convey integrated information from cerebellar PCs to the relay neuron in the vestibular nuclei, it is necessary to generate an AP in the axon initial segment of PCs. It is widely known that the ability to generate APs in a neuron is mainly determined by the intrinsic membrane excitability. In the field of cerebellum-dependent motor learning, there is accumulating evidence supporting the emerging hypothesis that the storage of motor memory may be achieved by the modulation of the intrinsic excitability [16, 30, 31, 38, 140]. My result suggests that cerebellar PCs are less excitable after the formation of OKR memory, which facilitates the decrease in cerebellar output through synergistic cooperation with the synaptic LTD in PCs (Figure 2.10).

GENERAL CONCLUSION

Of the experimental strategies to evaluate memory trace in the brain, observational studies are a primary approach because possible molecules, signaling pathways, neural plasticity, or neuronal ensemble can be identified as candidates for memory traces in the brain. In this dissertation, I performed two observational studies to suggest possible molecular and cellular traces for cerebellum-dependent motor memory. First, I successfully summarized a comprehensive cerebellar protein list related to cerebellum-dependent motor memory using a quantitative proteomic profiling technique. Second, I discovered the altered synaptic and intrinsic excitabilities in the cerebellar Purkinje cells after a formation of cerebellum-dependent motor memory. Convincing candidates from the result should lead to further investigations, such as loss-of-function or gain-of-function studies to validate the function as part of the internal representation of the motor memory. Consequently, I believe that this dissertation would be a potentially important resource for discovering unknown molecules or mechanisms underlying cerebellum-dependent motor memory.

Bibliography

1. Kandel, E.R., Y. Dudai, and M.R. Mayford, *The molecular and systems biology of memory.* Cell, 2014. **157**(1): p. 163-86.
2. Scoville, W.B. and B. Milner, *Loss of recent memory after bilateral hippocampal lesions.* J Neurol Neurosurg Psychiatry, 1957. **20**(1): p. 11-21.
3. Squire, L.R., *Memory and the hippocampus: a synthesis from findings with rats, monkeys, and humans.* Psychol Rev, 1992. **99**(2): p. 195-231.
4. Kandel, E.R., *The molecular biology of memory storage: a dialogue between genes and synapses.* Science, 2001. **294**(5544): p. 1030-8.
5. Josselyn, S.A. and S. Tonegawa, *Memory engrams: Recalling the past and imagining the future.* Science, 2020. **367**(6473): p. eaaw4325.
6. Tronson, N.C. and J.R. Taylor, *Molecular mechanisms of memory reconsolidation.* Nat Rev Neurosci, 2007. **8**(4): p. 262-75.
7. Jarome, T.J. and F.J. Helmstetter, *Protein degradation and protein synthesis in long-term memory formation.* Front Mol Neurosci, 2014. **7**: p. 61.
8. Josselyn, S.A. and P.W. Frankland, *Memory Allocation: Mechanisms and Function.* Annu Rev Neurosci, 2018. **41**: p. 389-413.
9. Lamprecht, R., et al., *Fear conditioning induces distinct patterns of gene expression in lateral amygdala.* Genes Brain Behav, 2009. **8**(8): p. 735-43.
10. Pontes, A.H. and M.V. de Sousa, *Mass Spectrometry-Based Approaches to Understand the Molecular Basis of Memory.* Front Chem, 2016. **4**: p. 40.
11. Dieterich, D.C. and M.R. Kreutz, *Proteomics of the Synapse--A Quantitative Approach to Neuronal Plasticity.* Mol Cell Proteomics, 2016. **15**(2): p. 368-81.
12. Disterhoft, J.F. and M.M. Oh, *Learning, aging and intrinsic neuronal plasticity.* Trends Neurosci, 2006. **29**(10): p. 587-99.
13. Bliss, T.V. and G.L. Collingridge, *A synaptic model of memory: long-term potentiation in the hippocampus.* Nature, 1993. **361**(6407): p. 31-9.
14. Neves, G., S.F. Cooke, and T.V. Bliss, *Synaptic plasticity, memory and the hippocampus: a neural network approach to causality.* Nat Rev Neurosci, 2008. **9**(1): p. 65-75.
15. Nabavi, S., et al., *Engineering a memory with LTD and LTP.* Nature, 2014. **511**(7509): p. 348-52.
16. Titley, H.K., N. Brunel, and C. Hansel, *Toward a Neurocentric View of Learning.* Neuron, 2017. **95**(1): p. 19-32.
17. Yousuf, H., et al., *Modulation of intrinsic excitability as a function of learning within the fear conditioning circuit.* Neurobiology of learning and memory, 2019. **167**: p. 107132.
18. Moyer, J.R., Jr., L.T. Thompson, and J.F. Disterhoft, *Trace eyeblink conditioning increases CA1 excitability in a transient and learning-specific manner.* J Neurosci, 1996. **16**(17): p. 5536-46.
19. McKernan, M.G. and P. Shinnick-Gallagher, *Fear conditioning induces a lasting potentiation of synaptic currents in vitro.* Nature, 1997. **390**(6660): p. 607-11.
20. Saar, D., Y. Grossman, and E. Barkai, *Reduced synaptic facilitation between pyramidal neurons in the piriform cortex after odor learning.* Journal of Neuroscience, 1999. **19**(19): p. 8616-8622.

21. Butler, C.W., et al., *Neurons Specifically Activated by Fear Learning in Lateral Amygdala Display Increased Synaptic Strength.* eNeuro, 2018. **5**(3): p. ENEURO.0114-18.2018.

22. Pignatelli, M., et al., *Engram Cell Excitability State Determines the Efficacy of Memory Retrieval.* Neuron, 2019. **101**(2): p. 274-284 e5.

23. Ito, M., *Long-term depression.* Annu Rev Neurosci, 1989. **12**(1): p. 85-102.

24. Gao, Z., B.J. van Beugen, and C.I. De Zeeuw, *Distributed synergistic plasticity and cerebellar learning.* Nat Rev Neurosci, 2012. **13**(9): p. 619-35.

25. D'Angelo, E., et al., *Distributed Circuit Plasticity: New Clues for the Cerebellar Mechanisms of Learning.* Cerebellum, 2016. **15**(2): p. 139-51.

26. Schreurs, B.G., J.V. Sanchez-Andres, and D.L. Alkon, *Learning-specific differences in Purkinje-cell dendrites of lobule HVI (Lobulus simplex): intracellular recording in a rabbit cerebellar slice.* Brain Res, 1991. **548**(1-2): p. 18-22.

27. Schreurs, B.G., et al., *Dendritic excitability microzones and occluded long-term depression after classical conditioning of the rabbit's nictitating membrane response.* J Neurophysiol, 1997. **77**(1): p. 86-92.

28. Schreurs, B.G., et al., *Intracellular correlates of acquisition and long-term memory of classical conditioning in Purkinje cell dendrites in slices of rabbit cerebellar lobule HVI.* J Neurosci, 1998. **18**(14): p. 5498-507.

29. Inoshita, T. and T. Hirano, *Occurrence of long-term depression in the cerebellar flocculus during adaptation of optokinetic response.* Elife, 2018. **7**.

30. Titley, H.K., et al., *Intrinsic Excitability Increase in Cerebellar Purkinje Cells after Delay Eye-Blink Conditioning in Mice.* J Neurosci, 2020. **40**(10): p. 2038-2046.

31. Jang, D.C., H.G. Shim, and S.J. Kim, *Intrinsic Plasticity of Cerebellar Purkinje Cells Contributes to Motor Memory Consolidation.* J Neurosci, 2020. **40**(21): p. 4145-4157.

32. Cavallaro, S., et al., *Gene expression profiles during long-term memory consolidation.* Eur J Neurosci, 2001. **13**(9): p. 1809-15.

33. Barmack, N.H., Z. Qian, and V. Yakhnitsa, *Long-term climbing fibre activity induces transcription of microRNAs in cerebellar Purkinje cells.* Philos Trans R Soc Lond B Biol Sci, 2014. **369**(1652).

34. Li, Y., et al., *Learning and reconsolidation implicate different synaptic mechanisms.* Proc Natl Acad Sci U S A, 2013. **110**(12): p. 4798-803.

35. Brito, V., et al., *Hippocampal Egr1-dependent neuronal ensembles negatively regulate motor learning.* bioRxiv, 2020: p. 2020.11.26.399949.

36. Ito, M., *Cerebellar circuitry as a neuronal machine.* Prog Neurobiol, 2006. **78**(3-5): p. 272-303.

37. Hirano, T., *Regulation and Interaction of Multiple Types of Synaptic Plasticity in a Purkinje Neuron and Their Contribution to Motor Learning.* Cerebellum, 2018. **17**(6): p. 756-765.

38. Shim, H.G., Y.S. Lee, and S.J. Kim, *The Emerging Concept of Intrinsic Plasticity: Activity-dependent Modulation of Intrinsic Excitability in Cerebellar Purkinje Cells and Motor Learning.* Exp Neurobiol, 2018. **27**(3): p. 139-154.

39. Marr, D., *A theory of cerebellar cortex.* J Physiol, 1969. **202**(2): p. 437-70.

40. Albus, J.S., *A theory of cerebellar function.* Mathematical Biosciences, 1971. **10**(1-2): p. 25-61.

41. Ito, M., *Cerebellar control of the vestibulo-ocular reflex--around the flocculus hypothesis.* Annu Rev Neurosci, 1982. **5**: p. 275-96.

42. Boyden, E.S., et al., *Selective engagement of plasticity mechanisms for motor memory storage.* Neuron, 2006. **51**(6): p. 823-34.

43. De Zeeuw, C.I., et al., *Expression of a protein kinase C inhibitor in Purkinje cells blocks cerebellar LTD and adaptation of the vestibulo-ocular reflex.* Neuron, 1998. **20**(3): p. 495-508.

44. Shutoh, F., et al., *Loss of adaptability of horizontal optokinetic response eye movements in mGluR1 knockout mice.* Neurosci Res, 2002. **42**(2): p. 141-5.

45. Aiba, A., et al., *Deficient cerebellar long-term depression and impaired motor learning in mGluR1 mutant mice.* Cell, 1994. **79**(2): p. 377-88.

46. van Alphen, A.M. and C.I. De Zeeuw, *Cerebellar LTD facilitates but is not essential for long-term adaptation of the vestibulo-ocular reflex.* Eur J Neurosci, 2002. **16**(3): p. 486-90.

47. Hansel, C., et al., *alphaCaMKII Is essential for cerebellar LTD and motor learning.* Neuron, 2006. **51**(6): p. 835-43.

48. Titley, H.K., R. Heskin-Sweezie, and D.M. Broussard, *The bidirectionality of motor learning in the vestibulo-ocular reflex is a function of cerebellar mGluR1 receptors.* J Neurophysiol, 2010. **104**(6): p. 3657-66.

49. Feil, R., et al., *Impairment of LTD and cerebellar learning by Purkinje cell-specific ablation of cGMP-dependent protein kinase I.* J Cell Biol, 2003. **163**(2): p. 295-302.

50. Katoh, A., et al., *Inhibition of nitric oxide synthesis and gene knockout of neuronal nitric oxide synthase impaired adaptation of mouse optokinetic response eye movements.* Learn Mem, 2000. **7**(4): p. 220-6.

51. Koekkoek, S.K., et al., *Cerebellar LTD and learning-dependent timing of conditioned eyelid responses.* Science, 2003. **301**(5640): p. 1736-9.

52. Boyden, E.S., A. Katoh, and J.L. Raymond, *Cerebellum-dependent learning: the role of multiple plasticity mechanisms.* Annu Rev Neurosci, 2004. **27**: p. 581-609.

53. Hansel, C., D.J. Linden, and E. D'Angelo, *Beyond parallel fiber LTD: the diversity of synaptic and non-synaptic plasticity in the cerebellum.* Nat Neurosci, 2001. **4**(5): p. 467-75.

54. Kakegawa, W., et al., *Optogenetic Control of Synaptic AMPA Receptor Endocytosis Reveals Roles of LTD in Motor Learning.* Neuron, 2018. **99**(5): p. 985-998 e6.

55. Boyden, E.S. and J.L. Raymond, *Active reversal of motor memories reveals rules governing memory encoding.* Neuron, 2003. **39**(6): p. 1031-42.

56. Tanaka, S., et al., *Long-term potentiation of inhibitory synaptic transmission onto cerebellar Purkinje neurons contributes to adaptation of vestibulo-ocular reflex.* J Neurosci, 2013. **33**(43): p. 17209-20.

57. Gutierrez-Castellanos, N., et al., *Motor Learning Requires Purkinje Cell Synaptic Potentiation through Activation of AMPA-Receptor Subunit GluA3.* Neuron, 2017. **93**(2): p. 409-424.

58. Katoh, A., et al., *Defective control and adaptation of reflex eye movements in mutant mice deficient in either the glutamate receptor delta2 subunit or Purkinje cells.* Eur J Neurosci, 2005. **21**(5): p. 1315-26.

59.   Kimpo, R.R. and J.L. Raymond, *Impaired motor learning in the vestibulo-ocular reflex in mice with multiple climbing fiber input to cerebellar Purkinje cells.* J Neurosci, 2007. **27**(21): p. 5672-82.

60.   Schonewille, M., et al., *Purkinje cell-specific knockout of the protein phosphatase PP2B impairs potentiation and cerebellar motor learning.* Neuron, 2010. **67**(4): p. 618-28.

61.   Galliano, E., et al., *Silencing the majority of cerebellar granule cells uncovers their essential role in motor learning and consolidation.* Cell Rep, 2013. **3**(4): p. 1239-51.

62.   Schonewille, M., et al., *Reevaluating the role of LTD in cerebellar motor learning.* Neuron, 2011. **70**(1): p. 43-50.

63.   Morrison, R.S., et al., *Proteomic analysis in the neurosciences.* Mol Cell Proteomics, 2002. **1**(8): p. 553-60.

64.   Woo, J., et al., *Quantitative Proteomics Reveals Temporal Proteomic Changes in Signaling Pathways during BV2 Mouse Microglial Cell Activation.* J Proteome Res, 2017. **16**(9): p. 3419-3432.

65.   Wulff, P., et al., *Synaptic inhibition of Purkinje cells mediates consolidation of vestibulo-cerebellar motor learning.* Nat Neurosci, 2009. **12**(8): p. 1042-9.

66.   Wang, W., et al., *Distinct cerebellar engrams in short-term and long-term motor learning.* Proc Natl Acad Sci U S A, 2014. **111**(1): p. E188-93.

67.   Ryu, C., et al., *STIM1 Regulates Somatic Ca(2+) Signals and Intrinsic Firing Properties of Cerebellar Purkinje Neurons.* J Neurosci, 2017. **37**(37): p. 8876-8894.

68.   Kim, Y.G., et al., *Kdm3b haploinsufficiency impairs the consolidation of cerebellum-dependent motor memory in mice.* Mol Brain, 2021. **14**(1): p. 106.

69.   Stahl, J.S., A.M. van Alphen, and C.I. De Zeeuw, *A comparison of video and magnetic search coil recordings of mouse eye movements.* J Neurosci Methods, 2000. **99**(1-2): p. 101-10.

70.   Kim, Y.G., et al., *Quantitative Proteomics Reveals Distinct Molecular Signatures of Different Cerebellum-Dependent Learning Paradigms.* J Proteome Res, 2020. **19**(5): p. 2011-2025.

71.   Huang da, W., B.T. Sherman, and R.A. Lempicki, *Bioinformatics enrichment tools: paths toward the comprehensive functional analysis of large gene lists.* Nucleic Acids Res, 2009. **37**(1): p. 1-13.

72.   Zhang, K., et al., *i-GSEA4GWAS: a web server for identification of pathways/gene sets associated with traits by applying an improved gene set enrichment analysis to genome-wide association study.* Nucleic Acids Res, 2010. **38**(Web Server issue): p. W90-5.

73.   Subramanian, A., et al., *Gene set enrichment analysis: a knowledge-based approach for interpreting genome-wide expression profiles.* Proc Natl Acad Sci U S A, 2005. **102**(43): p. 15545-50.

74.   Merico, D., et al., *Enrichment map: a network-based method for gene-set enrichment visualization and interpretation.* PLoS One, 2010. **5**(11): p. e13984.

75.   Langfelder, P. and S. Horvath, *WGCNA: an R package for weighted correlation network analysis.* BMC Bioinformatics, 2008. **9**: p. 559.

76.   Pfaffl, M.W., *A new mathematical model for relative quantification in real-*

time RT-PCR. Nucleic Acids Res, 2001. **29**(9): p. e45.

77. Lavallee-Adam, M., et al., *PSEA-Quant: a protein set enrichment analysis on label-free and label-based protein quantification data.* J Proteome Res, 2014. **13**(12): p. 5496-509.

78. Dityatev, A. and M. Schachner, *Extracellular matrix molecules and synaptic plasticity.* Nat Rev Neurosci, 2003. **4**(6): p. 456-68.

79. Dityatev, A., M. Schachner, and P. Sonderegger, *The dual role of the extracellular matrix in synaptic plasticity and homeostasis.* Nat Rev Neurosci, 2010. **11**(11): p. 735-46.

80. Wang, D. and J. Fawcett, *The perineuronal net and the control of CNS plasticity.* Cell Tissue Res, 2012. **349**(1): p. 147-60.

81. Thompson, E.H., et al., *Removal of perineuronal nets disrupts recall of a remote fear memory.* Proc Natl Acad Sci U S A, 2018. **115**(3): p. 607-612.

82. Wakita, R., et al., *Differential regulations of vestibulo-ocular reflex and optokinetic response by beta- and alpha2-adrenergic receptors in the cerebellar flocculus.* Sci Rep, 2017. **7**(1): p. 3944.

83. Pham, N.C., et al., *Differential effects of inferior olive lesion on vestibulo-ocular and optokinetic motor learning.* Neuroreport, 2020. **31**(1): p. 9-16.

84. Itoh, S., et al., *Neuronal plasticity in hippocampal mossy fiber-CA3 synapses of mice lacking the inositol-1,4,5-trisphosphate type 1 receptor.* Brain Res, 2001. **901**(1-2): p. 237-46.

85. Pratt, K.G., et al., *Presenilin 1 regulates homeostatic synaptic scaling through Akt signaling.* Nat Neurosci, 2011. **14**(9): p. 1112-4.

86. Gibson, H.E., et al., *A similar impairment in CA3 mossy fibre LTP in the R6/2 mouse model of Huntington's disease and in the complexin II knockout mouse.* Eur J Neurosci, 2005. **22**(7): p. 1701-12.

87. Shumyatsky, G.P., et al., *stathmin, a gene enriched in the amygdala, controls both learned and innate fear.* Cell, 2005. **123**(4): p. 697-709.

88. Cesca, F., et al., *The synapsins: key actors of synapse function and plasticity.* Prog Neurobiol, 2010. **91**(4): p. 313-48.

89. Winkle, C.C., et al., *Trim9 Deletion Alters the Morphogenesis of Developing and Adult-Born Hippocampal Neurons and Impairs Spatial Learning and Memory.* J Neurosci, 2016. **36**(18): p. 4940-58.

90. Hacohen-Kleiman, G., et al., *Activity-dependent neuroprotective protein deficiency models synaptic and developmental phenotypes of autism-like syndrome.* J Clin Invest, 2018. **128**(11): p. 4956-4969.

91. Lim, Y., et al., *alpha-Syn suppression reverses synaptic and memory defects in a mouse model of dementia with Lewy bodies.* J Neurosci, 2011. **31**(27): p. 10076-87.

92. Zhang, C., et al., *Presenilins are essential for regulating neurotransmitter release.* Nature, 2009. **460**(7255): p. 632-6.

93. Rizo, J. and T.C. Sudhof, *Snares and Munc18 in synaptic vesicle fusion.* Nat Rev Neurosci, 2002. **3**(8): p. 641-53.

94. Reim, K., et al., *Complexins regulate a late step in Ca2+-dependent neurotransmitter release.* Cell, 2001. **104**(1): p. 71-81.

95. Dorgans, K., et al., *Short-term plasticity at cerebellar granule cell to molecular layer interneuron synapses expands information processing.* Elife, 2019. **8**.

96. Burre, J., M. Sharma, and T.C. Sudhof, *Cell Biology and Pathophysiology*

of alpha-Synuclein. Cold Spring Harb Perspect Med, 2018. **8**(3).

97.   Ohkawa, N., et al., *The microtubule destabilizer stathmin mediates the development of dendritic arbors in neuronal cells.* J Cell Sci, 2007. **120**(Pt 8): p. 1447-56.

98.   Sugawara, T., et al., *Type 1 inositol trisphosphate receptor regulates cerebellar circuits by maintaining the spine morphology of purkinje cells in adult mice.* J Neurosci, 2013. **33**(30): p. 12186-96.

99.   Furuichi, T., et al., *Widespread expression of inositol 1,4,5-trisphosphate receptor type 1 gene (Insp3r1) in the mouse central nervous system.* Recept Channels, 1993. **1**(1): p. 11-24.

100.   Inoue, T., et al., *Type 1 inositol 1,4,5-trisphosphate receptor is required for induction of long-term depression in cerebellar Purkinje neurons.* Journal of Neuroscience, 1998. **18**(14): p. 5366-5373.

101.   Bourtchouladze, R., et al., *Different training procedures recruit either one or two critical periods for contextual memory consolidation, each of which requires protein synthesis and PKA.* Learning & Memory, 1998. **5**(4-5): p. 365-374.

102.   Cavallaro, S., et al., *Memory-specific temporal profiles of gene expression in the hippocampus.* Proc Natl Acad Sci U S A, 2002. **99**(25): p. 16279-84.

103.   Monopoli, M.P., et al., *Temporal proteomic profile of memory consolidation in the rat hippocampal dentate gyrus.* Proteomics, 2011. **11**(21): p. 4189-201.

104.   Morgado-Bernal, I., *Learning and memory consolidation: linking molecular and behavioral data.* Neuroscience, 2011. **176**: p. 12-9.

105.   Rao-Ruiz, P., et al., *Time-dependent changes in the mouse hippocampal synaptic membrane proteome after contextual fear conditioning.* Hippocampus, 2015. **25**(11): p. 1250-61.

106.   Ito, M., M. Sakurai, and P. Tongroach, *Climbing fibre induced depression of both mossy fibre responsiveness and glutamate sensitivity of cerebellar Purkinje cells.* J Physiol, 1982. **324**(Mar): p. 113-34.

107.   Salin, P.A., R.C. Malenka, and R.A. Nicoll, *Cyclic AMP mediates a presynaptic form of LTP at cerebellar parallel fiber synapses.* Neuron, 1996. **16**(4): p. 797-803.

108.   Lev-Ram, V., et al., *A new form of cerebellar long-term potentiation is postsynaptic and depends on nitric oxide but not cAMP.* Proc Natl Acad Sci U S A, 2002. **99**(12): p. 8389-93.

109.   Coesmans, M., et al., *Bidirectional parallel fiber plasticity in the cerebellum under climbing fiber control.* Neuron, 2004. **44**(4): p. 691-700.

110.   Jorntell, H. and C. Hansel, *Synaptic memories upside down: bidirectional plasticity at cerebellar parallel fiber-Purkinje cell synapses.* Neuron, 2006. **52**(2): p. 227-38.

111.   Hong, I., et al., *Quantitative proteomics of auditory fear conditioning.* Biochem Biophys Res Commun, 2013. **434**(1): p. 87-94.

112.   Borovok, N., et al., *Dynamics of Hippocampal Protein Expression During Long-term Spatial Memory Formation.* Mol Cell Proteomics, 2016. **15**(2): p. 523-41.

113.   Maurya, D.K., C.S. Sundaram, and P. Bhargava, *Proteome profile of whole cerebellum of the mature rat.* Proteomics, 2010. **10**(23): p. 4311-9.

114.   Yang, J.W., et al., *Proteome analysis of primary neurons and astrocytes from*

rat cerebellum. J Proteome Res, 2005. **4**(3): p. 768-88.

115.   McClatchy, D.B., et al., *Quantification of the synaptosomal proteome of the rat cerebellum during post-natal development.* Genome Res, 2007. **17**(9): p. 1378-88.

116.   Selimi, F., et al., *Proteomic studies of a single CNS synapse type: the parallel fiber/purkinje cell synapse.* PLoS Biol, 2009. **7**(4): p. e83.

117.   Corradini, E., et al., *Alterations in the cerebellar (Phospho)proteome of a cyclic guanosine monophosphate (cGMP)-dependent protein kinase knockout mouse.* Mol Cell Proteomics, 2014. **13**(8): p. 2004-16.

118.   Wang, X., et al., *Quantitative proteomic analysis of age-related subventricular zone proteins associated with neurodegenerative disease.* Sci Rep, 2016. **6**: p. 37443.

119.   Lee, B., et al., *The Possible Role of Neurobeachin in Extinction of Contextual Fear Memory.* Sci Rep, 2018. **8**(1): p. 13752.

120.   Mertins, P., et al., *iTRAQ labeling is superior to mTRAQ for quantitative global proteomics and phosphoproteomics.* Mol Cell Proteomics, 2012. **11**(6): p. M111 014423.

121.   McAlister, G.C., et al., *MultiNotch MS3 enables accurate, sensitive, and multiplexed detection of differential expression across cancer cell line proteomes.* Anal Chem, 2014. **86**(14): p. 7150-8.

122.   Savitski, M.M., et al., *Measuring and managing ratio compression for accurate iTRAQ/TMT quantification.* J Proteome Res, 2013. **12**(8): p. 3586-98.

123.   Pfammatter, S., E. Bonneil, and P. Thibault, *Improvement of Quantitative Measurements in Multiplex Proteomics Using High-Field Asymmetric Waveform Spectrometry.* J Proteome Res, 2016. **15**(12): p. 4653-4665.

124.   Liu, X., et al., *Optogenetic stimulation of a hippocampal engram activates fear memory recall.* Nature, 2012. **484**(7394): p. 381-5.

125.   Kim, Y.G. and S.J. Kim, *Decreased intrinsic excitability of cerebellar Purkinje cells following optokinetic learning in mice.* Mol Brain, 2020. **13**(1): p. 136.

126.   Kim, Y.G., J.J. Shin, and S.J. Kim, *Minhee Analysis Package: An Integrated Software Package for Detection and Management of Spontaneous Synaptic Events.* bioRxiv, 2021: p. 2021.05.27.443730.

127.   Kim, C.H., et al., *Lobule-specific membrane excitability of cerebellar Purkinje cells.* J Physiol, 2012. **590**(2): p. 273-88.

128.   Debanne, D., et al., *Paired-pulse facilitation and depression at unitary synapses in rat hippocampus: Quantal fluctuation affects subsequent release.* Journal of Physiology-London, 1996. **491**(1): p. 163-176.

129.   Hashimoto, K. and M. Kano, *Presynaptic origin of paired-pulse depression at climbing fibre Purkinje cell synapses in the rat cerebellum.* Journal of Physiology-London, 1998. **506**(2): p. 391-405.

130.   Sacco, T. and F. Tempia, *A-type potassium currents active at subthreshold potentials in mouse cerebellar Purkinje cells.* J Physiol, 2002. **543**(Pt 2): p. 505-20.

131.   Jung, S.C. and D.A. Hoffman, *Biphasic somatic A-type K channel downregulation mediates intrinsic plasticity in hippocampal CA1 pyramidal neurons.* PLoS One, 2009. **4**(8): p. e6549.

132.   Haghdoust, H., M. Janahmadi, and G. Behzadi, *Physiological role of*

dendrotoxin-sensitive K+ channels in the rat cerebellar Purkinje neurons. Physiol Res, 2007. **56**(6): p. 807-13.

133. Morgan, P.J., et al., *Kv1.1 contributes to a rapid homeostatic plasticity of intrinsic excitability in CA1 pyramidal neurons in vivo.* Elife, 2019. **8**: p. e49915.

134. Nagao, S., *Behavior of floccular Purkinje cells correlated with adaptation of horizontal optokinetic eye movement response in pigmented rabbits.* Exp Brain Res, 1988. **73**(3): p. 489-97.

135. Qiu, D.L. and T. Knopfel, *An NMDA receptor/nitric oxide cascade in presynaptic parallel fiber-Purkinje neuron long-term potentiation.* J Neurosci, 2007. **27**(13): p. 3408-15.

136. Qiu, D.L. and T. Knopfel, *Presynaptically expressed long-term depression at cerebellar parallel fiber synapses.* Pflugers Arch, 2009. **457**(4): p. 865-75.

137. Wang, Y.T. and D.J. Linden, *Expression of cerebellar long-term depression requires postsynaptic clathrin-mediated endocytosis.* Neuron, 2000. **25**(3): p. 635-47.

138. Xia, J., et al., *Cerebellar long-term depression requires PKC-regulated interactions between GluR2/3 and PDZ domain-containing proteins.* Neuron, 2000. **28**(2): p. 499-510.

139. Chen, L., et al., *The role of intrinsic excitability in the evolution of memory: Significance in memory allocation, consolidation, and updating.* Neurobiol Learn Mem, 2020. **173**: p. 107266.

140. Grasselli, G., et al., *SK2 channels in cerebellar Purkinje cells contribute to excitability modulation in motor-learning-specific memory traces.* PLoS Biol, 2020. **18**(1): p. e3000596.

국문요약

소뇌-의존적 운동 학습에 의해 유도된 소뇌 단백질 발현과 퍼킨지 세포 흥분성의 변화

김 용 규
서울대학교 대학원
의과대학 의과학과 (의과학전공)

신경 과학에서 뇌의 고등 기능 중에 하나인 학습과 기억이 어떤 분자 혹은 세포 기전에 의해 매개되는가 하는 것은 흥미로는 주제이다. 이 문제를 해결하기 위한 다양한 실험적 접근들 중에서 야생형 동물의 뇌에서 학습 이후 나타나는 흔적을 추적하는 일은 근본적으로 널리 사용되어오는 접근법이다. 학위과정동안 나는 소뇌-의존적 운동 기억이 소뇌의 분자적 그리고 세포 수준에서 남기는 흔적들에 대한 탐구를 진행하였다.

먼저 제1장에서는 소뇌-의존적 학습이 소뇌의 분자적 수준에서 남기는 흔적을 찾기 위한 시도를 하였다. 소뇌는 운동의 강도를 적절하게 조정하여 운동 능력을 향상시키는데, 기존 연구에 따르면 운동의 강도가 조절되는 방향에 따라 각각 다른 종류의 세포 기전이 존재할 수 있다는 가능성이 제기되었다. 기억의 형성과 유지에 있어서 새로운 단백질의 합성이 필수적이라는 사실을 고려하여, 나는 운동의 강도 조절 측면에서 서로 다른 방향의 운동 학습이 소뇌에서의 서로 다른 단백질군의 발현을 유도할 것이라는 가설을 세웠다.

나는 운동의 강도가 강해지거나 약해지는 방향으로 일어나는 서로 다른 3 가지 종류의 소뇌-의존적 안구 운동 학습을 겪은 생쥐에서 학습이 끝난 후 1 시간과 24 시간이 지난 소뇌에서 단백질 발현 수준을 단백체 프로파일링을 사용하여 정량하였다. 실험의 결과, 3 가지 학습

패러다임 학습 후 1 시간과 24 시간의 각 소뇌에서 총 43 개의 차발현 단백질을 발견하였다. 또한, 기능적 온톨로지 분석을 사용하여 세 가지 안구 운동 학습 후 24 시간이 지난 소뇌에서 통제군에 비해 발현이 증가하거나 감소한 단백질 그룹을 확인하였는데, 이 결과는 세 가지 안구 운동 기억의 형성에 있어서 별개의 생물학적 경로가 관여할 수 있음을 제안한다. 가중 상관 네트워크 분석을 실시하여 안구 운동 기억 학습량과 상관 관계가 있는 단백질 그룹을 발견하였다. 마지막으로, 이 단백질 그룹 중 4 가지 단백질(Snca, Sncb, Cttn 및 Stmn1)을 선택하여 단백체 프로파일링의 결과를 웨스턴블롯분석으로 검증하였다. 이 연구는 세 가지 소뇌 의존적 운동 학습 패러다임과 관련된 종합적인 단백질 목록을 제공하는데, 연구의 결과는 각 학습 패러다임이 소뇌에서 서로 구별되는 단백질군의 발현을 유도할 수 있다는 점을 시사한다.

제2장에서는 앞서 언급한 3 가지 학습 패러다임 중에서 시운동 반응 적응 현상을 가지고 진행한 연구이다. 시운동 반응은 시야의 움직임이 발생하면 이를 추종하는 반사적 안구 운동으로 망막에 안정된 물체의 상이 맺힐 수 있도록 돕는 역할을 한다. 시운동 반응은 환경의 변화에 따라 그 반응의 정도가 조절되는 특성을 가지는데, 이런 적응 과정에 소뇌가 관여한다. 소뇌에 존재하는 여러 신경세포들 중, 퍼킨지 세포는 소뇌 피질로 전달된 여러 감각 정보들을 통합하고 소뇌의 유일한 출력을 담당하는 것으로 알려져 있는데, 이와 같이 시운동 반응을 통제하는 신경 회로 상 퍼킨지 세포의 중요성에도 불구하고 시운동 반응 적응 학습 상황에서 소뇌 퍼킨지 세포의 전기생리학적 특성을 밝히려는 시도는 여전히 부족한 것이 사실이다. 따라서 본 연구에서 나는 시운동 적응 학습 이후 소뇌 퍼킨지 세포에서의 내재적 및 스냅스 흥분성의 변화가 유발되는지 여부를 확인하였다.

통제군과 50분의 시운동 학습을 마친 학습군에서 소뇌를 각각 얻은 후 퍼킨지 세포에서 전기생리학적 특성을 분석한 결과, 나는 학습군의 퍼킨지 세포에서 통제군에 비해 세포내 탈분극 전류 주입에 반응하여

나타나는 활동 전위의 발화율이 줄어들고, 레오베이스 전류가 커졌음을 발견하였다. 또한, 시운동 적응 학습은 시냅스 전 신경 전달 물질 소포의 방출 확률을 감소시킴으로써 소뇌 평행섬유와 퍼킨지 세포 사이의 흥분성 시냅스 전달을 약화시켰다. 2장의 연구 결과를 종합하면, 시운동 적응 학습은 소뇌 퍼킨지 세포의 내재적 및 시냅스 수준 모두에서 신경 흥분성의 약화를 유발하는데, 이는 소뇌-의존적 안구 운동 학습을 매개하는 다중 가소성의 존재 가능성을 시사한다.

이 논문에서 나는 소뇌-의존적 운동 기억이 소뇌의 분자 그리고 세포 수준에서 남기는 기억 흔적을 찾기 위해 두 가지의 관찰 연구를 수행하였다. 탐구와 분석을 통해 찾은 후보 단백질과 신경 가소성은 운동 기억 형성 및 고착화 과정에 실제로 관여하는지 여부를 검증하는 후속 연구로 이어져 할 것이다. 결론적으로, 이 논문은 소뇌-의존적 운동 기억을 매개하지만 기존에 알려져 있지 않은 분자 또는 신경 가소성의 발견을 촉진하는 중요한 자원이 될 수 있을 것이다.